Caspases switch off m^{6}A RNA modification pathway to reactivate a ubiquitous human tumor virus

Kun Zhang[1,2], Yucheng Zhang[3], Jun Wan[3,4,5] and Renfeng Li[1,2,6,7,8*]

[1]Philips Institute for Oral Health Research, School of Dentistry, Virginia Commonwealth University, Richmond, Virginia, 23298, USA

[2]Department of Oral and Craniofacial Molecular Biology, School of Dentistry, Virginia Commonwealth University, Richmond, Virginia, 23298, USA

[3]Department of Medical and Molecular Genetics, Indiana University School of Medicine, Indianapolis, Indiana, 46202, USA

[4]Center for Computational Biology and Bioinformatics, Indiana University School of Medicine, Indianapolis, Indiana, 46202, USA.

[5]Department of BioHealth Informatics, School of Informatics and Computing, Indiana University – Purdue University at Indianapolis, Indianapolis, Indiana, 46202, USA

[6]Department of Microbiology and Immunology, School of Medicine, Virginia Commonwealth University, Richmond, Virginia, 23298, USA

[7]Massey Cancer Center, Virginia Commonwealth University, Richmond, Virginia, 23298, USA.

[8]Lead Contact

[*]Corresponding author: rli@vcu.edu (RL)

Abstract

The methylation of RNA at the N6 position of adenosine (m^6A) orchestrates multiple biological processes to control development, differentiation, and cell cycle, as well as various aspects of the virus life cycle. How the m^6A RNA modification pathway is regulated to finely tune these processes remains poorly understood. Here, we discovered the m^6A reader YTHDF2 as a caspase substrate via proteome-wide prediction, followed by *in vitro* and *in vivo* validations. We further demonstrated that cleavage-resistant YTHDF2 blocks, while cleavage-mimicking YTHDF2 fragments promote, the replication of a common human oncogenic virus, Epstein-Barr virus (EBV). Intriguingly, our study revealed a feedback regulation between YTHDF2 and caspase-8 via m^6A modification of *CASP8* mRNA and YTHDF2 cleavage during EBV replication. Further, we discovered that caspases cleave multiple components within the m^6A RNA modification pathway to benefit EBV replication. Together, our study establishes that caspase disarming of the m^6A RNA modification machinery fosters EBV reactivation.

Keywords

Epstein-Barr virus, reactivation, lytic replication, restriction factor, m^6A RNA modification, YTHDF2, METTL3, METTL14, WTAP, caspase cleavage

Introduction

Epstein-Barr virus (EBV) is a ubiquitous tumor virus causing several types of cancer of B cell, T cell and epithelial cell origin (Young and Rickinson, 2004; Young et al., 2016). Globally, EBV infection causes more than 200,000 new cancer cases and 140,000 deaths per year (Cohen et al., 2011). The life cycle of EBV include a quiescent latent phase and an active replication phase (De

Leo et al., 2020). The switch from latency to lytic replication, also called reactivation, involves a series of signaling pathways that drive the expression of two EBV immediate early genes, *ZTA* and *RTA* (Kenney and Mertz, 2014). Host factors that restrict or promote the expression of *ZTA* and *RTA* determine the threshold for EBV lytic cycle activation (Kenney and Mertz, 2014; Lieberman, 2013; Lv et al., 2018; Zhang et al., 2017b). Oncolytic therapies based on reactivation of latent virus is a promising approach for targeted treatment of EBV-associated cancers (Fu et al., 2008), but these strategies require a deeper understanding of how the EBV life cycle is dynamically regulated by key cellular processes and pathways.

The N6-methyladenosine (m^6A) modification of viral and cellular mRNAs provides a novel mechanism of post-transcriptional control of gene expression (Manners et al., 2018; Meyer and Jaffrey, 2017; Williams et al., 2019). M^6A modification is dynamically regulated by methyltransferases (writers, METTL3/METTL14/WTAP/VIRMA) and demethylases (erasers, ALKBH5 and FTO) (Jia et al., 2011; Liu et al., 2014; Meyer and Jaffrey, 2017; Zheng et al., 2013). The m^6A-specific binding proteins (readers, e.g. YTHDF1/2/3 and YTHDC1/2) regulate various aspects of RNA function, including stability, splicing and translation (Manners et al., 2018; Meyer and Jaffrey, 2017; Shi et al., 2017; Wang et al., 2014). YTHDF2 mainly regulates mRNA decay through direct recruitment of the CCR4-NOT deadenylase complex (Du et al., 2016; Wang et al., 2014). Recent studies showed that YTHDF1 and YTHDF3 share redundant roles with YTHDF2 in RNA decay (Lasman et al., 2020; Zaccara and Jaffrey, 2020). All three YTHDF proteins undergo phase separation through binding to m^6A modified RNA (Fu and Zhuang, 2020; Ries et al., 2019; Wang et al., 2020).

The m^6A RNA modification pathway has been shown to promote or restrict virus infection and replication depending on the viral and cellular context (Courtney et al., 2017; Gokhale et al., 2016; Hesser et al., 2018; Imam et al., 2018; Kennedy et al., 2016; Lichinchi et al., 2016; Rubio et al., 2018; Tan et al., 2018; Tirumuru et al., 2016; Tsai et al., 2018; Winkler et al., 2018). For example, m^6A modification of cellular genes promotes human cytomegalovirus (HCMV) replication through downregulating the interferon pathway (Rubio et al., 2018). YTHDF2 binding to m^6A-modified viral RNA restricts Kaposi's sarcoma-associated herpesvirus (KSHV) and EBV replication through promoting RNA decay (Lang et al., 2019; Tan et al., 2018). Despite the key role of the m^6A pathway in virus life cycle, how this pathway is finely regulated during viral infection or reactivation remains largely unexplored.

Although caspase-mediated cell death is intrinsically hostile for viral replication, emerging studies from our group and others have demonstrated that caspase cleavage of cellular restriction factors promote EBV and KSHV reactivation (Burton et al., 2020; De Leo et al., 2017; Lv et al., 2018; Tabtieng et al., 2018; Zhang et al., 2017b). Based on two evolutionarily conserved cleavage motifs we discovered for PIAS1 during EBV reactivation (Zhang et al., 2017b), we screened the entire human proteome and identified 16 potential caspase substates that carry the same motifs. Among these proteins, we validated 5 out of 6 as *bona fide* caspase substrates and then focused on the m^6A reader YTHDF2 and, subsequently, the entire m^6A RNA modification pathway in the context of EBV reactivation process. We found that caspase-mediated cleavage converts YTHDF2 from a restriction factor to several fragments that promote EBV reactivation. Mechanistically, we demonstrated that YTHDF2 promotes the degradation of *CASP8* mRNA via m^6A modification to limit caspase activation and viral replication. Importantly, we further

illustrated that multiple m^6A pathway components, including methyltransferases and other readers, were also cleaved by caspases to promote viral replication. Together, these findings uncovered an unexpected cross-regulation between caspases and the m^6A RNA modification pathway in switching EBV from latency to rapid replication.

Results

Cleavage sequence-guided identification of potential novel host factors involved in EBV replication

Recently, our group demonstrated that PIAS1 is an EBV restriction factor that is cleaved by caspase-3, -6 and -8 to promote EBV replication (Zhang et al., 2017b). The two evolutionally conserved sequences surrounding PIAS1 cleavage site D100 and D433, (LTYD*G and NGVD*G), are quite different from the canonical caspase cleavage motifs (Julien and Wells, 2017). We predicted that other proteins within the cellular proteome may contain the same sequences and hence are potentially regulated by caspases. Using these two cleavage sequences to search the human proteome, we discovered 16 additional putative caspase substrates, including RNA binding proteins (YTHDF2 and EIF4H), chromatin remodeling proteins (MTA1 and EHMT2) and a SARS-CoV2 receptor ACE2 (**Figure 1A & 1B**).

We selected 6 candidates (YTHDF2, EIF4H, MAGEA10, SORT1, MTA1, and EHMT2) to monitor their stability in EBV-positive Akata cells upon anti-IgG-induced B cell receptor (BCR) activation, a process that triggers caspase activation and EBV reactivation (**Figure 1C**) (Lv et al., 2018; Lv et al., 2017; Zhang et al., 2017b). All 6 proteins were downregulated upon BCR activation but not SAMHD1, a cellular restriction factor against EBV replication (Zhang et al.,

2019). To further determine whether any of these proteins are regulated by caspase, we pre-treated the cells with a caspase-3/7 inhibitor or a pan-caspase inhibitor followed by IgG-crosslinking of BCR. We found that the downregulation of YTHDF2, MAGEA10, SORT1, MTA1, and EHMT2 was reversed by the caspase inhibition, suggesting that these proteins are *bona fide* caspase substrates in cells (**Figure 1D**). Caspase inhibition partially restored the EIF4H, indicating an involvement of other pathways in controlling EIF4H protein level (**Figure 1D**).

To determine whether any of these proteins play a role in EBV life cycle, we utilized a CRISPR/Cas9 genome editing approach to knock out the corresponding genes in Akata (EBV+) cells, and then evaluated the viral lytic gene products upon BCR stimulation. The depletion of YTHDF2 and EIF4H promoted EBV ZTA and RTA protein expression (**Figures 2A, 2B & S1A**). In contrast, the depletion of MAGEA10, SORT1, EHMT2 and MTA1 did not affect EBV protein expression (**Figure S1B-S1E**).

In addition, we demonstrated that YTHDF2 depletion promotes the expression of immediate-early, early and late genes even without lytic induction (**Figure 2C**), suggesting that YTHDF2 serves as a restriction factor against EBV reactivation in normal conditions. Due to the key role of m^6A RNA modification pathway in viral life cycle, we selected the m^6A reader YTHDF2 as a starting point to explore the regulation of this pathway by caspases in EBV replication.

YTHDF2 universally restricts EBV replication

YTHDF2 has been shown to promote or suppress KSHV lytic replication in a cell type-dependent manner, but mainly inhibit EBV replication in Burkitt lymphoma cells (Hesser et al., 2018; Lang et al., 2019; Tan et al., 2018) (**Figure 2B & 2C**). To investigate whether YTHDF2

has a unified function in EBV reactivation regardless of cell type and lytic induction methods, we knocked out YTHDF2 in another Burkitt lymphoma cell line P3HR-1 and a gastric cancer cell line SNU-719, respectively. We found that YTHDF2 depletion promoted EBV gene expression in both cell lines using two different lytic inducers (**Figure 2D-2F**), demonstrating a universal role of YTHDF2 in restricting EBV replication.

To further confirm the role of YTHDF2 in viral replication, we transduced the Akata (EBV+) cell with lentiviruses carrying control or the *YTHDF2* gene. YTHDF2 overexpression strongly inhibited EBV ZTA and RTA expression upon lytic induction (**Figure 2G**), and consequently abrogated the production of EBV progeny released to the medium (**Figure 2H**).

YTHDF2 is cleaved by caspase-3, -6 and -8 at two evolutionarily conserved sites

Having shown YTHDF2 as a caspase substrate during the course of EBV replication (**Figure 1B &1C**), we further observed a downregulation of YTHDF2 in Akata-4E3 (EBV-) cells upon IgG cross-linking, suggesting this physiologically relevant lytic trigger plays a major role in YTHDF2 destabilization (**Figure 3A**, YTHDF2 shorter exposure, lanes 4-6). In addition to the reduction of protein level, two putative cleaved fragments of YTHDF2 were observed, whose molecular weights (MWs) are 25 and 50 kDa, respectively (**Figure 3A**, YTHDF2 longer exposure).

As expected, caspase inhibition also blocked the generation of two fragments in both Akata (EBV+) and Akata-4E3 (EBV-) cells (**Figure 3B**, YTHDF2 longer exposure). We predicted that the 25 kDa fragment likely represents a C-terminal cleaved YTHDF2 (aa 368-579, predicted MW=24 kDa). Similarly, YTHDF2 was also downregulated in lytically induced P3HR-1 and

SNU-719 cells (**Figure S2A & S2B**). Caspase inhibition blocked YTHDF2 degradation (**Figure S2A & S2B**) and inhibited viral replication (Zhang et al., 2017b).

To determine the major caspases responsible for YTHDF2 cleavage, we performed an in vitro cleavage assay using individual recombinant caspases and YTHDF2. We found that caspase-3/-6/-8, and, to a lesser extent, caspase-7 all cleave YTHDF2 (**Figure S2C**). The sizes of cleaved fragments *in vitro* were similar to those observed in cells, suggesting that YTHDF2 is a *bona fide* caspase substrate *in vitro* and *in vivo*.

In addition to the predicted cleavage sites D367 (**Figures 1A**), we used an *in silico* prediction algorithm (CaspDB) to predict additional cleavage sites (Kumar et al., 2014). A second highest scoring cleavage site (D166) was identified near the N-terminal of YTHDF2 (**Figure 3C**).

To explore whether there are two cleavage sites in YTHDF2, we first generated an N-terminal V5-tagged YTHDF2 by a method we used previously for PIAS1 (Zhang et al., 2017b), which allows the determination of both N- and C-terminal cleavage fragments by anti-V5 and anti-YTHDF2 (C-terminal) monoclonal antibodies, respectively (**Figure 3D**). Given the sizes of these cleaved bands recognized by the C-terminal YTHDF2 antibody, we noticed that caspase-3, -6 and -8 mediated cleavage led to one ~50 kDa C-terminal fragment, and caspase-3, and to a lesser extend caspase-6 and -8, generated one 25 kDa C-terminal fragment (**Figure 3E**). The anti-V5 antibody revealed one ~50kDa N-terminal cleavage fragment generated by caspase-3 and one smaller N-terminal (slightly less than 25 kDa) fragment generated by all 3 caspases (**Figure 3F**). Together, these results demonstrate that YTHDF2 is indeed cleaved at two sites by caspase-3, -6 and -8.

To further confirm whether D166 and D367 are the major cleavage sites, we mutated these two residues to alanines (D166A/D367A) and then examined the cleavage profile using in vitro

cleavage assays (**Figure 3G & 3H**). Consistent with our prediction, mutations on those two sites prevented YTHDF2 cleavage by caspases, indicating that D166 and D367 are the major cleavage sites. To examine the conservation across different species of these two cleavage motifs (AMID*G and NGVD*G) within YTHDF2, we extracted 15 amino acids surrounding the cleavage sites from 80-97 vertebrate species. Interestingly, we found that not only the cleavage motifs but also the surrounding amino acids are highly conserved (**Figure 3I and Figure S2D**), suggesting a key regulatory function for YTHDF2 cleavage during evolution.

Considering cleavage sites are normally exposed to the surface of the protein, we used an I-TASSER (Iterative Threading ASSEmbly Refinement) algorithm (Yang and Zhang, 2015; Zhang et al., 2017a) to generate a 3-dimensional (3D) structure for full-length YTHDF2 by integrating the crystal structure of the YTH domain (Li et al., 2014; Zhu et al., 2014). One structure with two cleavage sites located on the protein surface was visualized with Chimera (Pettersen et al., 2004) and both sites fall within flexible regions favoring cleavage by caspases (**Figure 3J**).

Because caspase-3, -6 and -8 are the major caspases that can redundantly cleave YTHDF2 (**Figure S2C**) and another restriction factor PIAS1 (Zhang et al., 2017b), we created two *CASP3/CASP8/CASP6* (genes encoding caspase-3, -8 and -6) triply depleted Akata (EBV+) cell lines by CRISPR/Cas9 approaches. The depletion of these three caspases alleviated the degradation of YTHDF2 and PIAS1 upon lytic induction (**Figure 3K**; YTHDF2 and PIAS1 blots, lanes 2-3, 5-6 vs 8-9). Consequently, the accumulation of EBV immediate-early (IE) gene products ZTA and RTA was also significantly reduced (**Figure 3K**; ZTA and RTA blots, lanes 2-3, 5-6 vs 8-9). Interestingly, the depletion of caspase-3, -6 and -8 led to a slight increase of caspase-7 and -9 activation, which may contribute to the partial destabilization of YTHDF2 and PIAS1 upon lytic induction (**Figure 3K**; YTHDF2 and PIAS1 blots, lanes 1 vs 3 and 4 vs 6).

These results suggested that caspase-mediated cleavage of host restriction factors, YTHDF2 and PIAS1, promotes EBV lytic replication (Zhang et al., 2017b).

Caspase-mediated YTHDF2 cleavage promotes EBV replication

To further investigate whether caspase-mediated degradation of full length YTHDF2 abrogates its restriction toward EBV lytic replication, we first generated a CRISPR-resistant YTHDF2 variant in a lentiviral vector. The Akata (EBV+) YTHDF2-sg2 cell line was chosen because it allows creating a CRISPR-resistant YTHDF2 by introducing a silent mutation on the PAM sequence (**Figure 4A**) (Zhang et al., 2017b, 2019). After reconstituting the YTHDF2-depleted Akata (EBV+) cell with WT and mutant (D166A/D367A) YTHDF2 by lentiviral transduction, we measured YTHDF2 protein degradation, viral protein accumulation and viral DNA replication after lytic induction. YTHDF2 (D166A/D367A) mutant was resistant to caspase-mediated cleavage and therefore became more stable than the WT counterpart upon lytic induction (**Figure 4B**, lane 6 vs 9). Although both proteins strongly suppressed EBV protein accumulation and viral replication, the YTHDF2 (D166A/D367A) mutant exhibited a stronger anti-viral activity than that of the WT (**Figure 4B & 4C**), further consolidating caspase-mediated cleavage in antagonizing the anti-viral function of YTHDF2.

Caspase-mediated cleavage led to not only a decrease of total YTHDF2 protein level but also an increase of cleaved fragments (**Figure 3A & 3B**). We hypothesized that these cleavage fragments compete with WT YTHDF2 to promote viral replication. To test this hypothesis, we created a series of cleavage-mimicking fragments using a lentiviral vector (**Figure 4D**). We then transduced SNU-719 cells to establish individual cell lines. All these fragments promoted expression of EBV ZTA and RTA upon lytic induction in these gastric cancer cell lines (**Figure 4E**, lane 1 vs 2-6). To further confirm these results, we established fragment-expressing cell lines

using Akata (EBV+) cells. F2 (aa 1-367)-expressing cell line failed being established after multiple attempts. However, in other four cell lines established, these cleavage-mimicking fragments strongly promoted EBV ZTA and RTA expression (**Figure 4F**, lane 1 vs 2-5 and lane 6 vs 7-10).

YTHDF2 has been shown to bind CNOT1 to recruit CCR4-NOT deadenylase complex for RNA decay (Du et al., 2016). To determine whether YTHDF2 cleavage impairs its binding to CNOT1, we co-transfected a CNOT1-SH domain-expressing construct with individual YTHDF2 fragment-expressing vector into 293T cells and then performed a co-immunoprecipitation (co-IP) assay. As expected, we found that CNOT1 is co-IPed with WT YTHDF2 (**Figure 4G,** lane 1). We also observed weaker binding signals of CNOT1 with F2 (aa 1-367), F4 (aa 167-579) and F5 (aa 368-579) fragments, compared to full-length YTHDF2 (**Figure 4G,** lane 1 vs 3, 5 & 6). This is in part consistent with a previous study showing that YTHDF2 (aa 100-200) binds to CNOT1 (Du et al., 2016). However, our study indicated that the YTH domain coordinates with the N-terminal region for enhanced YTHDF2 binding to CNOT1. Interestingly, two fragments, F1 (aa 1-166) and F3 (aa 167-367), lost the interaction with CNOT1, suggesting an essential N-terminal binding site for CNOT1 locating near the caspase cleavage site D166 of YTHDF2 (**Figure 4G,** lane 3 vs 2 & 4). Together, these results suggested that caspase mediated cleavage could convert YTHDF2 from an anti-viral restriction factor to several pro-viral fragments (**Figure 4H**).

YTHDF2 regulates viral and cellular gene stability to promote viral replication

It is known that YTHDF2 binds to m^6A-modified viral and cellular RNAs to control their stability (Hesser et al., 2018; Manners et al., 2018; Tan and Gao, 2018; Wang et al., 2014). By m^6A RNA immunoprecipitation (RIP) followed by reverse transcription quantitative real-time PCR (RT-qPCR) analysis, we found that EBV immediate early (*ZTA/BZLF1* and *RTA/BRLF1*)

and early (*BGLF4*) transcripts are modified by m^6A, not only revealing a new m^6A target *BGLF4* but also confirming the results for *ZTA and RTA* captured by m^6A-sequencing (m^6A-seq) analyses (Lang et al., 2019) (**Figure S3A**). We further demonstrated that YTHDF2 strongly binds to *ZTA*, *RTA* and *BGLF4* transcripts given the results from YTHDF2 RIP coupled with RT-qPCR analysis (**Figure S3B**). Together, all these results suggested that YTHDF2 binds to EBV lytic transcripts through m^6A modifications (**Figure S3**) and then promotes their decay to restrict EBV reactivation (**Figure 2C & 2E**).

In addition to regulating viral mRNA stability, YTHDF2 was reported to modulate m^6A-modified cellular transcripts to affect a variety of cellular processes. YTHDF2 targets were identified by YTHDF2 RIP and PAR-CLIP (photoactivatable ribounucleoside crosslinking and immunoprecipitation) datasets from previous publications (Fei et al., 2020; Wang et al., 2014). We found a group of YTHDF2 target genes involved in the biological process of "activation of cysteine-type endopeptidase activity involved in apoptotic process", also known as "caspase activation" (**Figure S4A**). Majority of these proteins have protein-protein interactions with caspase-8 (CASP8). As caspase activation plays a critical role in promoting EBV reactivation (**Figure 3K**) (Zhang et al., 2017b), we reasoned that YTHDF2 may regulate these genes to foster viral replication. The RT-qPCR results revealed that the mRNA levels of many potential YTHDF2 targets were elevated after YTHDF2 was knocked out by CRISPR/Cas9. Particularly, *CASP8* (encoding caspase-8) had more than 2-fold significant increase in both Akata (EBV+) and P3HR-1 cells (**Figure 5A & 5B**).

To test whether *CASP8* is modified by m^6A in EBV-positive cells, we performed m^6A RIP followed by RT-qPCR using Akata (EBV+) cells. The results demonstrated that *CASP8* mRNA is strongly modified by m^6A, compared to the controls (**Figure 5C**). In addition, YTHDF2

indeed bound to *CASP8* mRNA as revealed YTHDF2 RIP-qPCR analysis (**Figure 5D**). Consistent with mRNA elevation, caspase-8 protein level was also increased upon YTHDF2 depletion (**Figure 5E-5G** lanes 1, 3 vs 5). Upon lytic induction, we observed enhanced caspase-8 activation and consequently PIAS1 degradation (**Figure 5E-5G,** lanes 2, 4 vs 6). Conversely, YTHDF2 reconstitution led to reduced caspase-8 protein level and caspase activation upon lytic induction (**Figure S4B,** lanes 1-3 vs 4-6 & 7-9). To further understand the relationship between YTHDF2 regulation of caspase-8 and EBV replication, we pre-treated the YTHDF2-depleted Akata (EBV+) cells with or without a caspase-8 inhibitor. We found that caspase-8 inhibition reduces EBV ZTA and RTA expression and consequently inhibits EBV virion production even when YTHDF2 is depleted (**Figure S4C & S4D,** lane 2 vs 3 & lane 5 vs 6). Therefore, the depletion of YTHDF2 can promote viral reactivation partially through enhanced capase-8 activation.

M^6A modifications are mainly located near the stop codon region to regulate mRNA decay (Dominissini et al., 2012; Meyer et al., 2012; Wang et al., 2014). By mining the m^6A modification database (Liu et al., 2015; Liu et al., 2018) and YTHDF2-PAR-CLIP datasets (Wang et al., 2014), we found that *CASP8*-Exon-7 has the highest m^6A peaks that are closed to the stop codon (**Figure 5H**). Using conserved m^6A motif DRACH (D=G/A/U, R=G/A, H=A/U/C) (Linder et al., 2015), we identified 15 potential m^6A sites that are evenly distributed across the entire Exon-7 (**Figure 5H**). We found that Motif-2 (M2), M3, M5, M8 and M12 are highly conserved across more than 90 vertebrates ranging from human, mouse, bat to zebrafish, while the others likely evolve gradually during evolution (**Figure 5I and Table S3**).

To determine whether m^6A modifications contribute to *CASP8* mRNA stability, we synthesized the Exon-7 DNA of WT *CASP8* [without the first 20 base bases (bps)], and its mutant counterparts with conserved motifs (M2, M3, M5, M8 and M12) or all putative motifs mutated (**Figure 5J**). Luciferase reporters were created with WT or mutant DNA inserted into the 3'-untranslated region (3'-UTR) of an m^6A-null vector (**Figure 5J**). These reporters were modified to silently mutate all putative m^6A sites in the *Renillia* and *Firefly luciferase* genes to specifically test the function of m^6A modifications on *CASP8*-Exon-7 (Gokhale et al., 2020). We then transfected these plasmids individually into SNU-719 cells carrying YTHDF2 or with YTHDF2 depleted by CRISPR/Cas9. Disruption of m^6A modification by mutations enhanced the relative luciferase activity compared to the WT reporter (**Figure 5K**). In addition, depletion of YTHDF2 also enhanced the relative luciferase activity (**Figure 5K**), suggesting that YTHDF2 directly regulates *CASP8* stability. We also noticed a further enhancement of relative luciferase activity for mutant reporters in YTHDF2 depleted cells (**Figure 5K**), suggesting a regulation of *CASP8* stability by additional m^6A readers, e.g. YTHDF1 or YTHDF3 (Zaccara and Jaffrey, 2020).

Together, these results suggested that YTHDF2 depletion by CRISPR/Cas9 or its cleavage by caspases could promote viral reactivation through up-regulating caspase-8 which further enhances the cleavage of antiviral restriction factors, including PIAS1 and YTHDF2 (**Figure 5L**) (Zhang et al., 2017b).

M^6A pathway proteins are regulated by caspase-mediated cleavage.

The m^6A RNA modification machinery contains writers, readers and erasers that mediate methylation, RNA binding and demethylation steps, respectively (**Figure 6A**). Prompted by our YTHDF2 results, we predicted that other members involved in the m^6A pathway may be

downregulated by caspase-mediated cleavage during viral replication. To evaluate this possibility, we first monitored the protein levels of additional m^6A readers (YTHDF1, YTHDF3, YTHDC1 and YTHDC2), m^6A writers (METTL3, METTL14, VIRMA and WTAP), and m^6A erasers (ALKBH5 and FTO). Interestingly, except ALKBH5, all other proteins were significantly down-regulated upon lytic induction (**Figures 6B & S5A-S5K**). As a control, the protein level of a putative DNA N6-methyladenine (6mA) writer N6AMT1 did not change upon lytic induction (**Figures 6B & S5L**), suggesting a specific regulation of the m^6A RNA modification pathway by cellular caspases.

To further demonstrate the role of caspases in the downregulation of m^6A pathway proteins, we examined their protein levels in the presence of caspase-3/7 or pan-caspase inhibitors. Indeed, we found that caspase inhibition could restore the protein levels of YTHDF1, YTHDF3, METTL14, WTAP, VIRMA, and FTO (**Figure 6C**). The partial restoration of YTHDC1, YTHDC2, and METTL3 suggested that these proteins are controlled partially by caspase cleavage and partially by other protein degradation mechanisms (**Figure 6C**).

YTHDF2 shares high sequence homology with YTHDF1 and YTHDF3. Sequence alignment showed that the cleavage motif AMID*G, but not NGVD*G, is partially conserved among YTHDF family proteins (**Figure S6A**). Because TVVD*G in YTHDF1 and AITD*G in YTHDF3 are also evolutionary conserved (**Figure S6B & S6C**), we reasoned that YTHDF1 and YTHDF3 are subjected to caspase mediated cleavage on the N-terminal sites. Consistent with our prediction, not only did YTHDF1 and YTHDF3 protein levels decrease, a cleaved band near 50 kDa was generated upon lytic induction by IgG-crosslinking, matching the calculated molecular weights of C-terminal fragments generated by cleavage on the N-terminal sites

(**Figure S5B & S5C**). In addition, cleaved fragments were detected for YTHDC1, YTHDC2, METTL14, VIRMA and FTO (**Figure S5D-S5K**).

To further demonstrate that the m^6A writers are cleaved by caspase, we performed in vitro cleavage assay using purified proteins. Interestingly, we found that METTL14 is mainly cleaved by caspase-2, -5, and -6 revealed by anti-METTL14 antibody (**Figure 6D**), whereas WTAP is mainly cleaved by caspase-6 (**Figure 6E**). However, we only observed trace amount of METTL3 cleavage by caspase-4, -5, -6 and -7 revealed by anti-METTL3 antibody (**Figure S7A**).

The cleavage patterns suggested that METTL14 is cleaved on multiple sites while WTAP is possibly cleaved on one major site near the C-terminus (**Figure 6E**). Based on the C-terminal fragment molecular weight (15 kDa), we reasoned that D301 or D302 is cleaved. To examine this, we generated WTAP mutants (D301A and D301A/D302A) and performed in vitro cleavage experiments. Interestingly, only the D301A/D302A mutant could block WTAP cleavage (**Figure S7B**), indicating D302 as the major cleavage site. Sequence analysis revealed that the core cleavage motif TEDD*F is evolutionarily conserved (**Figure S7C**). Compared to cleavage sites normally followed by glycine, serine or alanine (Julien and Wells, 2017), the discovery of a conserved phenylalanine after the cleavage site extends our knowledge on the substrates recognition by caspase (**Figure S7D**).

Depletion of m^6A writers (METTL3, METTL14, WTAP or VIRMA) and reader YTHDF3 promotes EBV replication.

The aforementioned studies suggest that YTHDF2 restricts viral replication through m^6A modifications. We reasoned that the disruption of the m^6A writer complex and other readers might also promote viral replication. To test our hypothesis, we used a CRISPR/Cas9 genomic editing approach to deplete METTL3, METTL14, VIRMA and WTAP in Akata (EBV+) cells. Consistent with our prediction, depletion of METTL3, METTL14, VIRMA and WTAP all facilitated the expression of EBV ZTA and RTA (**Figure 7A, 7B & 7D**, lanes 2, 3, 5, 6 vs 8-9; **Figure 7C**, lanes 2, 4, 6 vs 8). Because YTHDF1 and YTHDF3 share redundant role with YTHDF2, we knocked out these two genes using CRISPR/Cas9 genomic editing approaches. Interestingly, depletion of YTHDF3 rather than YTHDF1 promoted EBV ZTA and RTA expression (**Figures 7E and S7E**). In addition, depletion of the major m^6A eraser ALKBH5 did not affect EBV protein accumulation (**Figure S7F**). All results together suggested that, in addition to m^6A readers, disruption of the m^6A writer complex by caspases further fosters EBV reactivation upon lytic induction (**Figure 7F**).

Discussion

Caspase activation and m^6A RNA modification pathway have documented essential roles in viral infections. However, it is unknown whether caspases regulate any members of the m^6A machinery to foster viral infection. Our study established an elegant regulation model about multiple members of the m^6A RNA modification pathway by caspase mediated cleavage, which play a crucial role in regulating the reactivation of EBV (**Figure 7F**).

In this study, we first identified 16 putative caspase substrates by searching the human proteome database using two unique cleavage motifs derived from PIAS1 (**Figure 1**). The m^6A reader

YTHDF2 was selected for in-depth analysis considering its critical role in the life cycle of diverse viruses, including EBV and KSHV (**Figures 2**) (Hesser et al., 2018; Lang et al., 2019; Tan et al., 2018).

Consistent with our prediction, YTHDF2 was indeed cleaved on D367 within the NGVD*G motif shared with PIAS1. Moreover, we discovered a second cleavage site (D166) within the motif AMID*G that is unique for YTHDF2 and not present in any other human proteins (**Figure 3**). Both cleavage sites, especially D166, are evolutionarily conserved across a diverse group of vertebrates ranging from human to zebrafish, highlighting that maintaining these cleavage sites during evolution is important for normal cellular processes (**Figures 3 and S2**).

In addition to YTH domain binding to m^6A, YTHDF2 contains a low complexity domain with disorder-promoting amino acids in the N-terminal and central parts. Our 3D structure modeling on full-length YTHDF2 clearly shows two cleavage sites on the surface area with flexible turns (**Figure 3J**). Because the low complexity domain is responsible for YTHDF2-mediated phase separation to form liquid droplets with high concentration of protein and RNA (Fu and Zhuang, 2020; Ries et al., 2019; Wang et al., 2020), our predicted protein structure model will provide valuable insights into the regulation of YTHDF family proteins under normal conditions.

The importance of the YTHDF2 cleavage in EBV replication is further supported by the following observations. First, cleavage-resistant YTHDF2 strongly inhibits EBV replication upon lytic induction. Second, overexpression of cleavage-mimicking YTHDF2 fragments promoted the accumulation of EBV immediate-early proteins. Finally, the interaction between YTHDF2 and CNOT1 was diminished upon caspase-mediated cleavage of YTHDF2, limiting the efficient recruitment of CCR4-NOT complex by YTHDF2 (**Figure 4**).

Although YTHDF2 regulation of viral transcripts stability contributes to viral replication (**Figures 2 & S3**) (Hesser et al., 2018; Lang et al., 2019; Tan et al., 2018), the extent to which cellular gene regulation by YTHDF2 plays in this process has been largely unexplored. By analyzing YTHDF2 targets transcripts we identified *CASP8* as a putative YTHDF2 target involved in EBV replication (**Figures 5 and S4**). We demonstrated that the *CASP8* transcript is modified by m^6A and bound by YTHDF2 and that depletion of YTHDF2 promotes *CASP8* mRNA level, caspase-8 protein level, and hence its activation and subsequent cleavage of PIAS1 favoring EBV lytic replication (**Figure 5**).

Intriguingly, we found 15 putative m^6A sites within the second to last exon. Among them, 5 sites are conserved across a diverse group of species. Although DNA sequences differ significantly across species, our discovery of conserved m^6A sites in regulating *CASP8* stability highlights the importance of m^6A RNA modification in controlling the basal levels of key cellular genes during evolution (**Figure 5**). The importance of caspase-8 activation in YTHDF2-depleted cells was further supported by the evidence that caspase-8 inhibition blocks PIAS1 degradation and EBV replication (**Figure S4**). Therefore, our discovery of *CASP8* mRNA targeting by YTHDF2 and YTHDF2 cleavage by caspase-8 has established an elegant feedback regulation mechanism controlling the switch of EBV from latent to lytic phase (**Figure 5**).

Importantly, our work on YTHDF2 led to the discovery of multiple m^6A RNA modification pathway proteins as caspase substrates and EBV restriction factors. The extension of YTHDF2 to YTHDF1 and YTHDF3 as caspase substrates was readily revealed by sequence alignment and cleavage patten analyses (**Figures S5 & S6**).

We provided compelling evidence that METTL14 and WTAP are cleaved by cellular caspases (**Figures 6 & S7**). Interestingly, WTAP is predominately cleaved by caspase-6 on D302 within

an evolutionarily conserved motif that differs significantly from canonical cleavage motifs (**Figure S7**). The cleavage pattern of METTL14 suggested that multiple sites are cleaved, possibly including D29 (EASD*S) revealed by a large scale proteomics study (Mahrus et al., 2008). It will be interesting to identify all cleavage sites on METTL14 and examine how specific cleavage contributes to the EBV latency and reactivation in the future. Importantly, the discovery of new cleavage motifs (**Figures S6 & S7**) would also guide us to discover novel caspase substrates using the motif searching method (**Figure 1**) and to determine the biological function of protein cleavage in viral life cycle and normal cellular processes.

In summary, our work has illustrated the value of a motif-based searching approach for the discovery of novel caspase substrates that are critical for viral replication. We have uncovered a unique caspase regulation mechanism for the m^6A RNA modification pathway, which is essential for the reactivation of a ubiquitous tumor virus. The discovery of conserved caspase cleavage motifs will guide us to discover novel caspase substrates with broad biological significance, provide valuable insights into the regulation of viral life cycle, and illuminate the key molecular mechanisms controlling normal cellular processes and disease progression.

STAR*Methods

Contact for Reagent and Resource Sharing

Further information and requests for resources and reagents should be directed to and will be fulfilled by the Lead Contact, Renfeng Li (rli@vcu.edu).

Experimental Model and Subject Details

Cell Lines and Cultures

The Akata (EBV+) and Akata-4E3 (EBV-), P3HR-1 and SNU-719 cells were cultured in RPMI 1640 medium supplemented with 10% FBS (Cat# 26140079, Thermo Fisher Scientific) in 5% CO_2 at 37°C. 293T cells were cultured in DMEM medium supplemented with 10% FBS (Cat# 26140079, Thermo Fisher Scientific) in 5% CO_2 at 37 °C.

Methods Details

Plasmids Construction

Halo-V5-YTHDF2 (full length and truncation mutants), Halo-V5-METTL13, Halo-V5-METTL14 and Halo-V5-WTAP were cloned into pHTN HaloTag CMV-neo vector (Cat# G7721, Promega) using Gibson assembly methods as previously described (Zhang et al., 2017b, 2019). Halo-V5-YTHDF2 mutant (D166A/D367A) and Halo-V5-WTAP mutants (D301A and D301A/D302A) were generated using the QuikChange II site-directed Mutagenesis Kit (Stratagene) following the manufacturer's instructions. All primers are listed in **Table S1**.

Target Gene Depletion by CRISPR/Cas9 Genome Editing

To deplete YTHDF2, EIF4H, MAGEA10, SORT1, MTA1, EHMT2, METTL3, METTL14, WTAP, VIRMA, YTHDF1, YTHDF3 and ALKBH5, two or three different sgRNAs were designed and cloned into lentiCRISPR v2-Puro vector (a gift from Feng Zhang; Addgene plasmid # 52961) (Sanjana et al., 2014) or lentiCRISPR v2-Blast vector (a gift from Mohan Babu, Addgene plasmids #83480) or lentiCRISPR v2-Hygro vector vector (a gift from Joshua Mendell, Addgene plasmids #91977) (Golden et al., 2017). Packaging 293T cells were

transfected with targeted gene sgRNAs or negative control (non-targeting sgRNA-NC) and helper vectors (pMD2.G and psPAX2; gifts from Didier Trono; Addgene plasmid #s 12259 and 12260, received via Yue Sun) using Lipofectamine 2000 reagent (Cat# 11668019, Life Technologies). Medium containing lentiviral particles and 8 mg/mL polybrene (Sigma-Aldrich, St. Louis) was used to infect Akata (EBV+) cells, P3HR-1 cells and SNU-719 cells. The stable cell lines were selected and maintained in RPMI medium supplemented with 2 μg/mL puromycin, 100 μg/mL hygromycin, or 10 μg/mL blasticidin.

To knockout three caspases (CASP3/CASP8/CASP6), first, one sgRNA targeting CASP3 (CASP3-sg1) was cloned into lentiCRISPR v2-Puro vector and Akata (EBV+) cells were used to create a CASP3-depleted cell line, Akata (EBV+)-CASP3-sg1, by CRISPR/Cas9 (puromycin-resistant). Second, one sgRNA targeting CASP8 (CASP8-sg1) and one control sgRNA(sg-NC) were cloned into lentiCRISPR v2-Blast vector. The constructs were packaged, and lentiviral particles were used to infect Akata (EBV+)-CASP3-sg1 and control Akata (EBV+)-sg-NC cells to generate Akata (EBV+)-CASP3-sg1/CASP8-sg1 and Akata (EBV+)-sg-NC/sg-NC cell lines. Third, two different sgRNAs targeting CASP6 (CASP6-sg1 and CASP6-sg2) and one control sgRNA (sg-NC) were designed and cloned into lentiCRISPR v2-Hygro vector. The constructs were packaged, and lentiviral particles were used to infect Akata (EBV+)-CASP3-sg1/CASP8-sg1 and control Akata (EBV+)-sg-NC/sg-NC cell line. The established Akata (EBV+)-CASP3-sg1/CASP8-sg1/CASP6-sg1, Akata (EBV+)-CASP3-sg1/CASP8-sg1/CASP6-sg2, and control Akata (EBV+)-sg-NC/sg-NC/sg-NC were maintained in RPMI medium supplemented with 100 μg/mL hygromycin, 2 μg/mL puromycin and 10 μg/mL blasticidin. The target guide RNA sequences are listed in **Table S1**.

Lentiviral Transduction of YTHDF2

The pLenti-C-Myc-DDK-P2A-BSD and pCMV6-Entry-YTHDF2 were purchased from Origene. The specific variants were generated by site-directed mutagenesis in pCMV6-Entry-YTHDF2 using the QuikChange II site-Directed Mutagenesis Kit (Cat# 200521, Stratagene) according to the manufacturer's instructions. The truncated YTHDF2 were cloned into pCMV6-Entry vector using Gibson assembly methods as we previous described (Zhang et al., 2017b, 2019). Subsequently, the WT, mutated and truncated YTHDF2 in pCMV6-Entry vector were digested using AsiSI and MluI and subcloned into the pLenti-C-Myc-DDK-P2A-BSD vector. To prepare lentiviruses, 293T cells were transfected with lentiviral vector containing the target gene and the help vectors (pMD2.G and psPAX2) using Lipofectamine 2000 reagent. The supernatants were collected 48 hs post-transfection to infect Akata (EBV+) cells or SNU-719 cells and then stable cell lines were selected in medium containing 10 μg/mL blasticidin.

Lytic Induction and Cell Treatment

For lytic induction in Akata (EBV+) cell lines, the cells were treated with IgG (1:200, Cat# 55087, MP Biomedicals) for 24 and 48 hrs. Akata-4E3(EBV-) cells were treated similarly as controls. To induce the EBV lytic cycle in P3HR-1 cells, the cells were triggered with TPA (20 ng/ml) and sodium butyrate (3 mM) for 24 hrs. For EBV lytic replication, the SNU-719 cells were treated with gemcitabine (1 μg/mL) or TPA (20 ng/ml) for 24 and 48 hrs. For caspase inhibition assay, cells were untreated or pretreated with caspase inhibitors (50 μM) for 1 hrs and then treated with IgG (1:200, Cat# 55087, MP Biomedicals) for additional 48 hrs.

Cell Lysis and Immunoblotting

Cell lysates were prepared in lysis buffer supplemented with protease inhibitors (Roche) as described previously. Protein concentration was determined by Bradford assay (Biorad). The proteins were separated on 4-20% TGX gels (Biorad) and transferred to PVDF membranes using semi-dry transfer system. Membranes were blocked in 5% milk and probed with primary and horseradish peroxidase-conjugated secondary antibodies.

Protein Expression and Purification

Halo-V5-YTHDF2 (WT and D166/D367A mutant), Halo-V5-METTL3, Halo-V5-METTL14 and Halo-V5-WTAP (WT, D301A and D301/D302A mutants) proteins were expressed and purified as previously described (Li et al., 2015). Briefly, Halo-tagged plasmids were transfected into 293T cells at 50-60% confluence. Two T175 flasks of transfected cells were harvested 48 hrs post-transfection at 100% confluence and lysed with 25 ml HaloTag Protein Purification Buffer (50 mM HEPES pH7.5, 150 mM NaCl, 1mM DTT, 1mM EDTA and 0.005% NP40/IGEPAL CA-630) with Protease Inhibitor Cocktail. Halo-V5-tagged proteins were enriched using the Halo-tag resin and proteins were eluted from the resin by washing 3 times with 0.5 ml HaloTag Protein Purification Buffer containing 20 µl Halo-TEV protease. The eluted proteins were stored at -80 °C for further use.

Reverse transcription and quantitative PCR (RT-qPCR)

Total RNA was isolated from cells with Isolate II RNA Mini Kit (Bioline) according to the manufacturer's instructions. Total RNA was reverse transcribed into cDNA using the High Capacity cDNA Reverse Transcription Kit (Invitrogen). qPCR was performed using Brilliant

SYBR Green qPCR master mix (Agilent Technology) with specific primers listed in **Table S1**. The relative expression of target mRNA was normalized by *β-actin* or *HPRT1* expression level.

EBV DNA Detection

To measure EBV replication, cell associated viral DNA and virion-associated DNA were determined by qPCR analysis. For intracellular viral DNA, total genomic DNA was extracted using the Genomic DNA Purification Kit (Cat# A1120, Promega). For extracellular viral DNA, the supernatant was treated with RQ1 DNase at 37 °C for 1 hr , deactivation by RQ1 DNase stop solution, followed by releasing virion associated DNA with proteinase and SDS treatment as previously described (Lv et al., 2018). The DNA was then purified by phenol/chloroform/isoamyl alcohol extraction. The relative viral DNA copy numbers were determined by qPCR using primers to *BALF5* gene. The reference gene *β-actin* was used for data normalization.

***In vitro* Caspase Cleavage Assay**

Purified V5-YTHDF2 (WT and mutants), V5-WTAP (WT and mutants), WT V5-METTL3 and WT V5-METTL14 were incubated with individual caspase in caspase assay buffer (50 mM HEPES, pH7.2, 50 mM NaCl, 0.1% Chaps, 10 mM EDTA, 5% Glycerol and 10mM DTT) at 37 °C for 2 hrs with gentle agitation. Reactions were stopped by boiling in 2x SDS sample buffer and samples were analyzed by Western blot.

Immunoprecipitation (IP) Assay

293T cells (50-60% confluence) were co-transfected with Halo-V5 tagged WT or truncated YTHDF2 and HA tagged CNOT1-SH domain using Lipofectamine 2000. The cells were harvested 48 hrs post-transfection and lysed in RIPA lysis buffer (50 mM Tris-HCl, 150 mM NaCl, 1% NP40, 1% deoxycholate, 0.1% SDS and 1 mM EDTA) containing protease inhibitor cocktail (Cat# 11836153001, Roche) and phosphatase inhibitors (1 mM Na_3VO_4 and 1 mM NaF). The IP was carried out as previously described (Zhang et al., 2017b, 2019).

RNA-binding Protein Immunoprecipitation

RNA-binding protein immunoprecipitation (RIP) was performed using a Magna RIP kit (Cat# 17-700, Millipore) according to the manufacturer's protocol. Briefly, Akata (EBV+) cells were either untreated or treated by IgG cross-linking for 24 hrs and then lysed with RIP lysis buffer from the kit. A part of the lysate (10%) was saved as input. The beads were washed with RIP wash buffer, followed by incubation with YTHDF2 antibody (Proteintech, 24744-1-AP) for 30 mins at room temperature and then washed twice with RIP wash buffer. The cell lysate was incubated with antibody-coated beads overnight at 4 °C. The next day, the beads were collected and washed six times with RIP wash buffer. The enriched RNA-protein complex was treated with proteinase K and the released RNA was purified using phenol-chloroform extraction and reverse transcribed for further qPCR analysis using primers listed in **Table S1**.

M^6A-RNA Immunoprecipitation (m^6A RIP) Assay

Total RNA was extracted from Akata (EBV+) cells (untreated or treated by IgG cross-linking for 24 hrs) by TRIzol (Cat# 1596026, Thermo Scientific) and then treated with RQ1 DNase (Cat# M6101, Promega) at 37 °C for 30 mins, followed by RNA re-extraction using TRIzol. 40 μL

protein A/G magnetic beads (Thermo Scientific, 88802) were blocked in 1% BSA solution for 2 h, followed by incubation with 10 μg of anti-m^6A antibody (Millipore, ABE572) at 4 °C for 1 h with rotation. 300 μg purified RNA was added to the antibody-bound beads in IP buffer containing 10 mM Tris-HCL at pH 7.4, 50mM NaCl and 0.1% NP-40 supplemented RNasin plus RNase inhibitor (Cat# N2611, Promega) and incubated overnight at 4 °C with rotation. The same RNA aliquot was used as input. The beads were washed three times with IP buffer, and RNA was eluted twice with IP buffer containing 6.67 mM m^6A salt (Cat# M2780, Sigma-Aldrich) (200 μL for each elution). The elutes were pooled together and then purified with phenol-chloroform extraction. The immunoprecipitated RNA was reverse transcribed to cDNA for qPCR analysis. The primers were listed in **Table S1**.

Reporter Cloning and Luciferase Assay

To generate *CASP8*-Exon-7 reporters, we used a psiCheck2 m^6A-null vector, in which all putative m^6A sites in the *Renillia* and *Firefly luciferase* genes were mutated (Gokhale et al., 2020). The WT *CASP8*-Exon-7, m^6A Mut1 (5 conserved m^6A sites were mutated to T) and Mut2 (all putative m^6A sites were mutate to T) DNA fragments were synthesized using gBlocks (IDT) and were cloned into psiCheck2 m^6A null vector by Gibson assembly methods using primers and templates listed in **Table S1**.

For luciferase assay, SNU-719 cells and SNU-719 YTHDF2-KD cells were seeded in 12-well plates prior to transfection. The cells were transfected with *CASP8*-Exon-7 luciferase reporters using Lipofectamine 2000 reagent. Forty-eight hours post-transfection, cell extracts were harvested and measured using the Dual-Luciferase assay kit (Promega). Each condition was performed in triplicate.

Bioinformatic Analysis

The 'multiz100way' alignment prepared from 100 vertebrate genomes was downloaded from UCSC Genome Browser (http://hgdownload.cse.ucsc.edu/goldenpath/hg38/multiz100way/). The nucleotide sequences around motifs of YTHDF1, YTHDF2, YTHDF3, and WTAP were extracted from 'multiz100way' alignment by maf_parse of the Phast package (Hubisz et al., 2011). The corresponding protein amino acid sequences of each motif were inferred based on the nucleic acid sequence alignments. Sequences containing frameshifting indels were discarded for amino acid alignment to avoid ambiguity. Motif logos were then generated by the WebLogo3 (Crooks et al., 2004).

To analyze the conservation of *CASP8*-Exon-7, we downloaded the phastCons 100-way conservation scores from 100 vertebrate genomes aligned to the human genome (http://hgdownload.cse.ucsc.edu/goldenpath/hg19/phastCons100way/). Given the m^6A motif (DRACH), we obtained 15 putative m^6A motif sequences within human *CASP8*-Exon 7 while extracting corresponding sequences from 100 species. After removing sequences containing deletions within the m^6A motif, we generated 15 motif logos by using the R package ggseqlogo (Wagih, 2017).

Quantification and Statistical Analysis

Statistical analyses employed a two-tailed Student's t test using Microsoft Excel software for comparison of two groups. A p value less than 0.05 was considered statistically significant.

Values were given as the mean ± standard deviation (SD) of biological or technical replicate experiments as discussed in figure legends.

Figures and Figure Legends

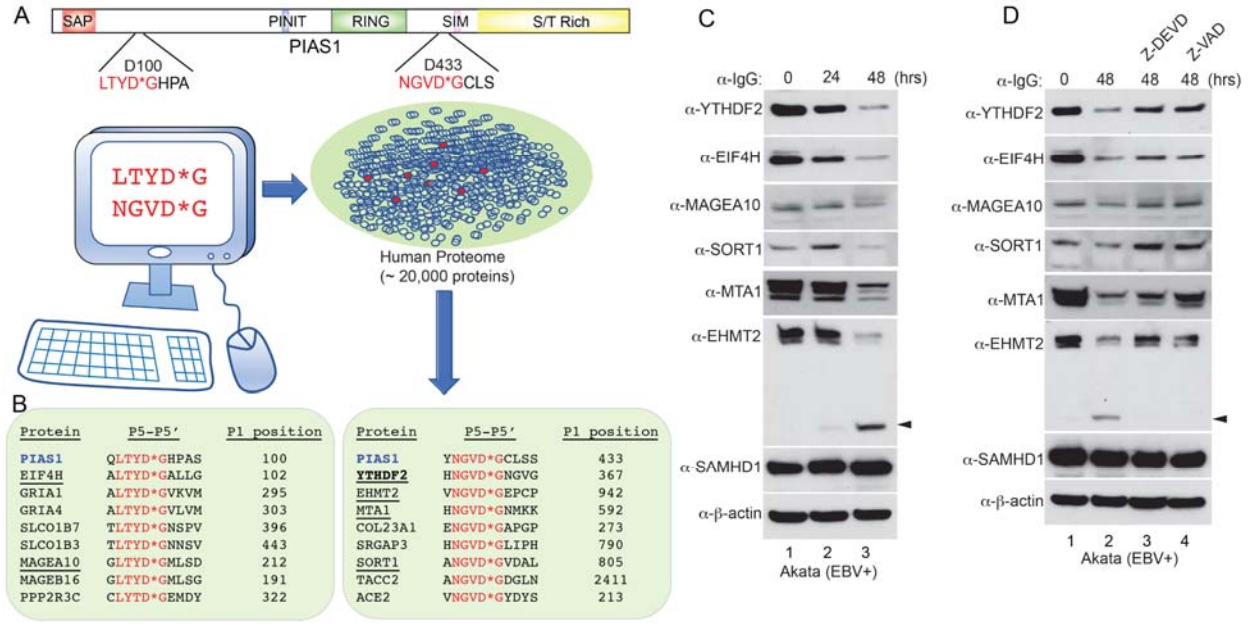

Figure 1. Identification of new potential caspase substrates during EBV reactivation.

(A) The cleavage motifs derived from PIAS1 (LTYD*G and NGVD*G) were used to virtually screen the entire human proteome for proteins sharing the same sequences. The human proteome dataset containing approximately 20,000 human protein-coding genes represented by the canonical protein sequence was downloaded from UniProtKB/Swiss-Prot.

(B) 16 additional proteins were extracted from the screen. 8 proteins carry the LTYD*G motif (left) and 8 proteins carry the NGVD*G motif (right). 6 proteins (underlined) were selected for further validation.

(C) Protein downregulation during EBV reactivation. Akata (EBV+) cells was treated with anti-IgG antibody to induce EBV reactivation for 0, 24 and 48 hrs. Western Blot showing the downregulation of 6 selected proteins using antibodies as indicated. SAMHD1 and β-actin were included as controls. Arrowhead denotes the cleaved fragment for EHMT2.

(D) Caspase inhibition blocks the degradation of YTHDF2, MAGEA10, SORT1 MTA1 and EHMT2. The Akata (EBV+) cells were either untreated or pretreated with a caspase-3/-7 inhibitor (Z-DEVD-FMK, 50 μM) or pan-caspase inhibitor (Z-VAD-FMK, 50 μM) for 1 hr, and then anti-IgG antibody was added for 48 hrs. Western Blot showing the protein levels of 6 selected proteins using antibodies as indicated. SAMHD1 and β-actin were included as controls. Arrowhead denotes cleaved EHMT2 fragment.

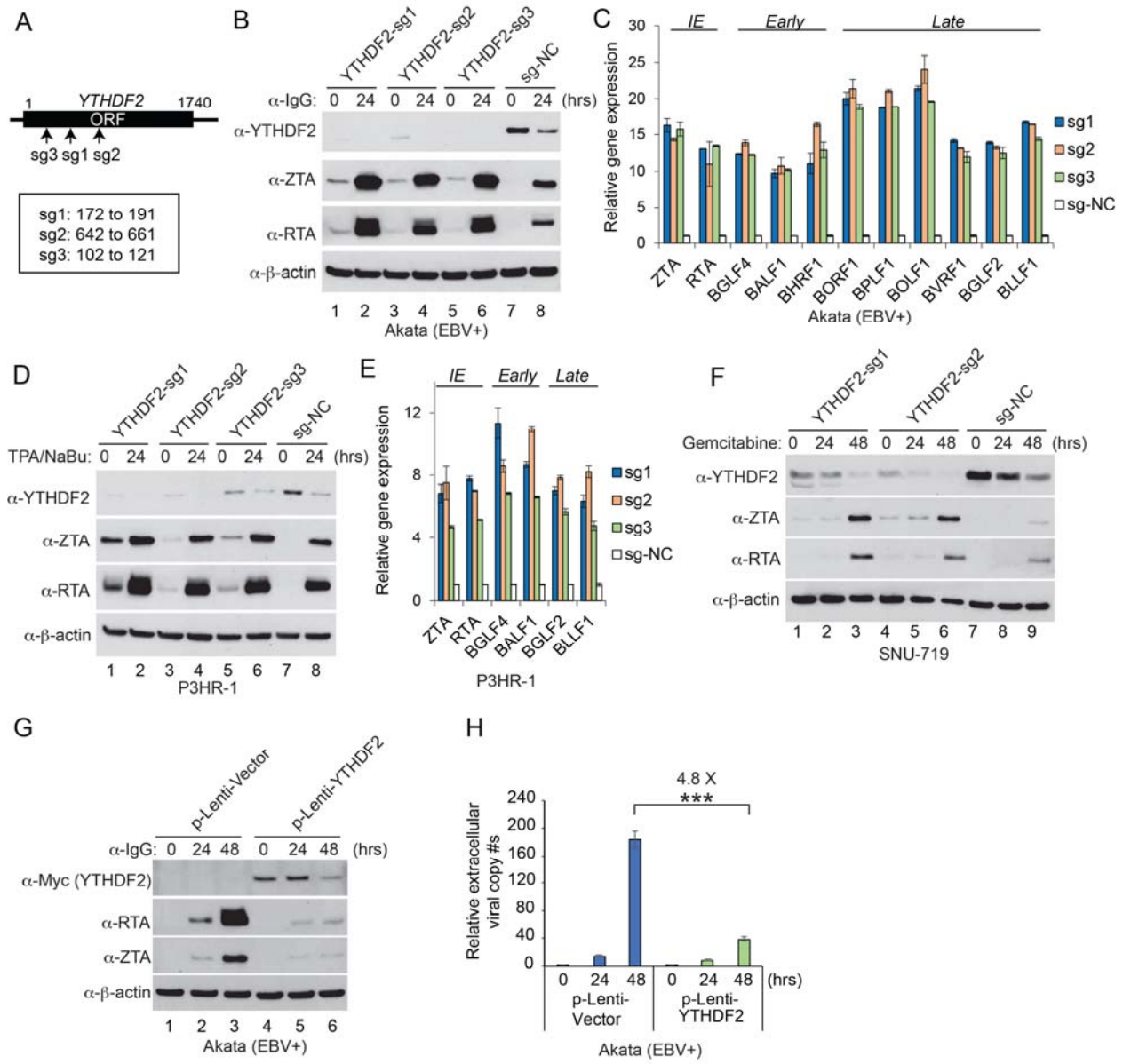

Figure 2. YTHDF2 restricts EBV reactivation.

(A) Schematic representation showing the relative positions of Cas9 target sites for small guide RNAs sg-1 to sg-3.

(B) Akata (EBV+) cells were used to establish stable cell lines using 3 different sgRNA constructs and a non-targeting control (sg-NC). The cells were untreated or lytically induced with anti-IgG-mediated cross-linking of BCR. YTHDF2 and viral protein expression levels were monitored by Western Blot using antibodies as indicated.

(C) RNAs from YTHDF2-depleted and control Akata cells were extracted and analyzed by RT-qPCR. The values of control were set as 1. Error bars indicate ±SD. IE, immediate early gene; Early, early gene; Late, late gene.

(D) P3HR-1 cells were used to establish stable cell lines as indicated. The cells were either untreated or treated with TPA and sodium butyrate (NaBu) to induce lytic reactivation. YTHDF2 and viral protein expression levels were monitored by Western Blot using antibodies as indicated.

(E) RNAs from YTHDF2-depleted and control P3HR-1 cells were extracted and analyzed by RT-qPCR. The values of control were set as 1. Error bars indicate ±SD. IE, immediate early gene; Early, early gene; Late, late gene.

(F) SUN-719 cells were used to establish stable cell lines as indicated. The cells were either untreated or treated with Gemcitabine to induce lytic reactivation. YTHDF2 and viral protein expression levels were monitored by Western Blot using antibodies as indicated.

(G) Akata (EBV+) cells were used to establish control and YTHDF2 overexpression cell line as indicated. The cells were untreated or lytically induced by anti-IgG treatment. The expression of YTHDF2 as monitored by an anti-Myc antibody. Viral protein expression levels were monitored by Western Blot using antibodies as indicated.

(H) Extracellular virion-associated DNA from cells treated in panel G was extracted and the relative EBV viral copy numbers were calculated by q-PCR analysis. The value of vector control

at 0 hr was set as 1. Results from three biological replicates are presented. Error bars indicate ±SD. ***, $p<0.001$.

See also Figure S1.

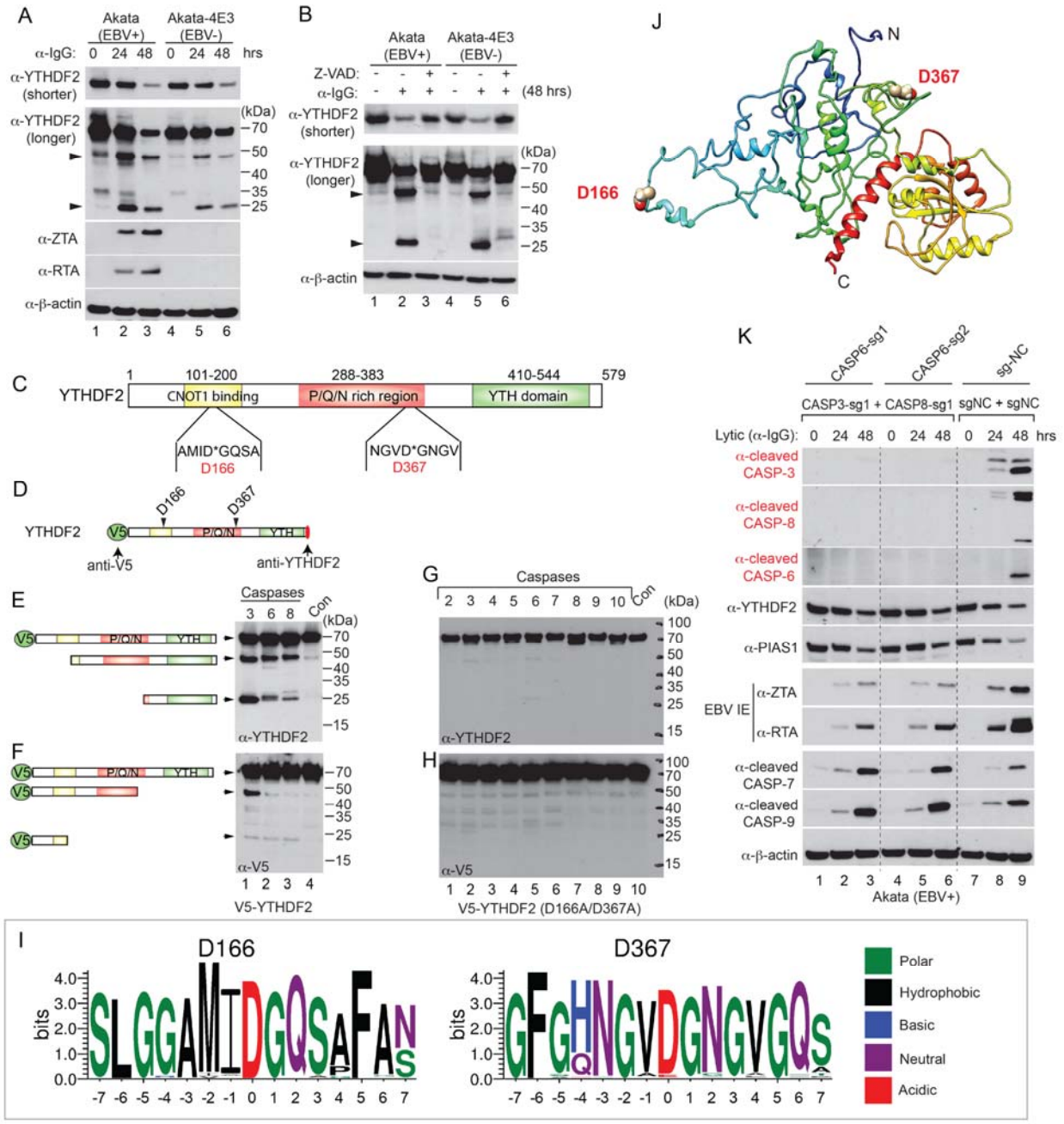

Figure 3. YTHDF2 is cleaved by caspases *in vivo* and *in vitro*.

(A) Western Blot showing YTHDF2 downregulation by IgG cross-linking induced BCR activation. Akata (EBV+) and Akata-4E3 (EBV-) cells were treated with anti-IgG antibody as indicated. YTHDF2 and viral protein expression levels were monitored by Western Blot. Arrowheads denote cleaved YTHDF2 in the longer exposure blot.

(B) Caspase inhibition blocks YTHDF2 degradation. The cells were either untreated or pretreated with a pan-caspase inhibitor (Z-VAD-FMK, 50 μM) for 1 hr, and then anti-IgG antibody was added for 48 hrs. Arrowheads denote cleaved YTHDF2.

(C) Functional domains and putative cleavage sites in YTHDF2. CaspDB was used to predict the potential cleavage sites in YTHDF2. The locations of the putative cleavage sites D166 and D367 were labeled as indicated. CNOT1 binding domain: responsible for the degradation of associated RNA; P/Q/N rich region: aggregation-prone region; YTH domain: responsible for binding to m^6A-modified RNA.

(D) Schematic representation of V5-tagged YTHDF2 with two putative cleavage sites. Red oval, anti-YTHDF2 monoclonal antibody recognition site.

(E-F). Wild-type V5-YTHDF2 was incubated with individual recombinant caspase for 2 hrs. Western Blot was performed using either anti-YTHDF2 (E) or anti-V5 (F) antibodies. The relative position of predicted cleavage fragments was labeled as indicated.

(G-H) YTHDF2 (D166A/D367A) mutant protein was incubated with individual recombinant caspase for 2 hrs. Western Blot was performed using antibodies as indicated.

(I) Motif analysis showing the conservation of the two cleavage sites and the surrounding amino acids. Amino acid sequences were extracted from 97 (D166) and 80 (D367) vertebrate species and motif logos were generated using WebLogo.

(J) Structure modeling of full-length YTHDF2 by I-TASSER. The two cleavage sites D166 and D367 are labeled as indicated. N and C denote N-terminus and C-terminus, respectively.

(K) Triple depletion of caspase-3, -8 and -6 reduces YTHDF2 and PIAS1 degradation and blocks viral protein accumulation. The CASP3/CASP8/CASP6-triply-depleted Akata (EBV+) cells

were lytically induced by anti-IgG treatment. The expression of cleaved caspases, YTHDF2, PIAS1 and viral proteins was monitored by Western Blot using antibodies as indicated.

See also Figure S2 and Table S2.

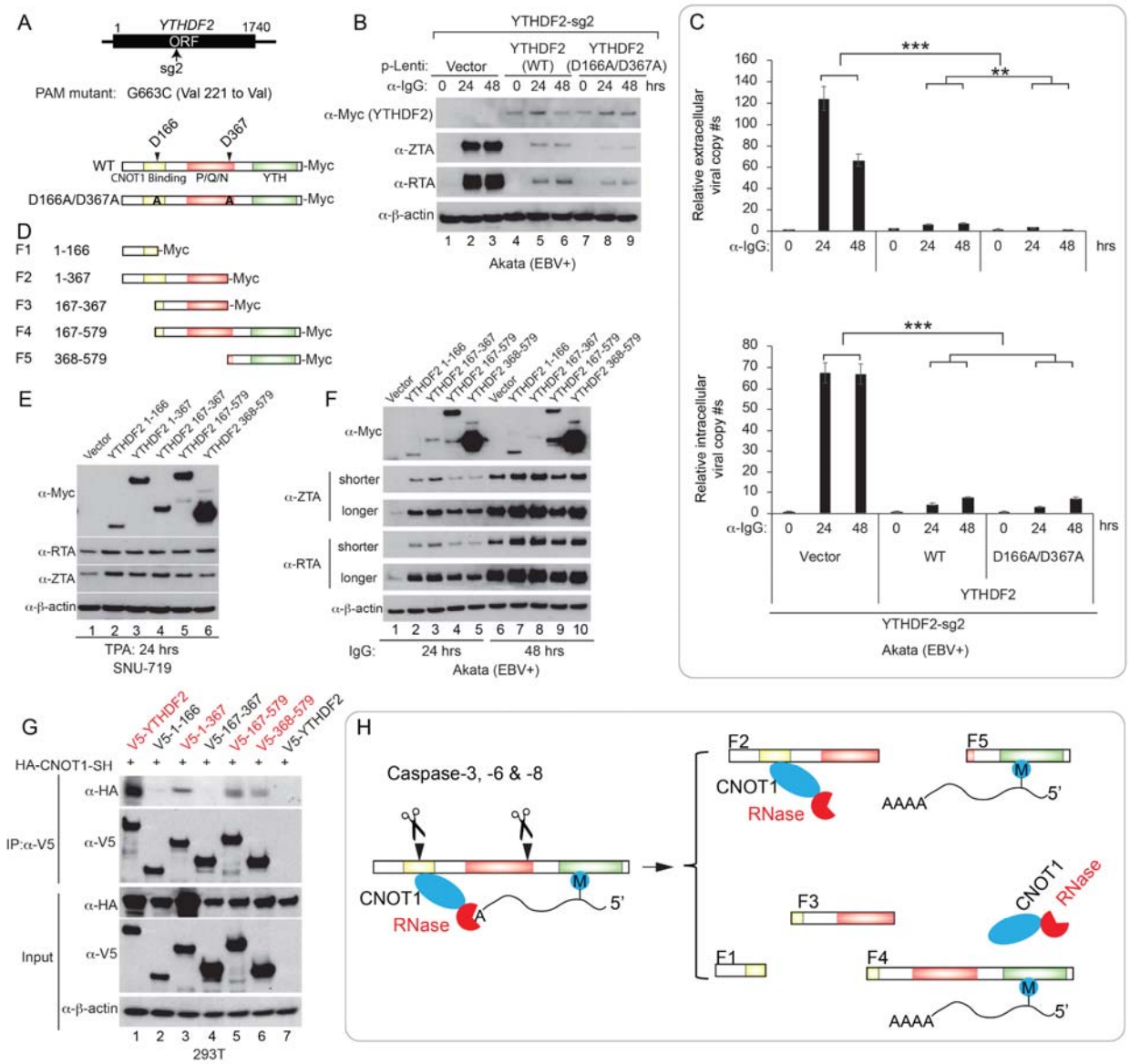

Figure 4. YTHDF2 cleavage promotes EBV replication.

(A) The design of CRISPR/Cas9-resistant YTHDF2 variant was based on the sg-2 protospacer adjacent motif (PAM). D166A/D367A mutations were introduced into the PAM-mutated YTHDF2. Both constructs were cloned into a lentiviral vector with a C-terminal Myc-tag.

(B-C) WT and cleavage-resistant YTHDF2 suppresses EBV replication. Akata (EBV+) YTHDF2-sg2 cells were reconstituted with WT or cleavage-resistant YTHDF2 (D166A/D367A) using lentiviral constructs. Western Blot analysis showing YTHDF2 and EBV protein expression

levels in these cell lines upon IgG cross-linking as indicated (B). Extracellular and intracellular viral DNA was measured by qPCR using primers specific to BALF5 (C). The value of vector control at 0 hr was set as 1. Results from three biological replicates are presented. Error bars indicate ±SD. **, $p<0.01$; ***, $p<0.001$.

(D) Schematic representation of 5 YTHDF2 cleavage-mimicking fragments. These fragments were cloned into a lentiviral vector with a C-terminal Myc-tag.

(E) SNU-719 cells were transduced with lentiviruses carrying vector control or individual fragment to establish stable cell lines. Western Blot analysis showing YTHDF2 fragments and EBV protein expression levels in these cell lines upon lytic induction by adding TPA (20 ng/ml) for 24 hrs.

(F) Akata (EBV+) cells were transduced with lentiviruses carrying vector control or individual fragment to establish stable cell lines. Western Blot analysis showing YTHDF2 fragments and EBV protein expression levels in these cell lines upon lytic induction by anti-IgG treatment for 24 and 48 hrs. Shorter and longer exposures were included to show the differences in protein levels.

(G) Caspase-mediated cleavage impairs YTHDF2 binding to CNOT1. Halo-V5-tagged WT YTHDF2 and the individual fragments were co-transfected with HA-tagged CNOT1 SH domain into 293T cells as indicated. Co-immunoprecipitation (Co-IP) experiments were performed using anti-V5 antibody-conjugated magnetic beads. The immunoprecipitated samples and total cell lysates (Input) were analyzed by Western Blot with antibodies as indicated.

(H) Model showing the functional consequences of YTHDF2 cleavage in CNOT1 binding and the targeting of m^6A-modified RNA.

See also Figure S4.

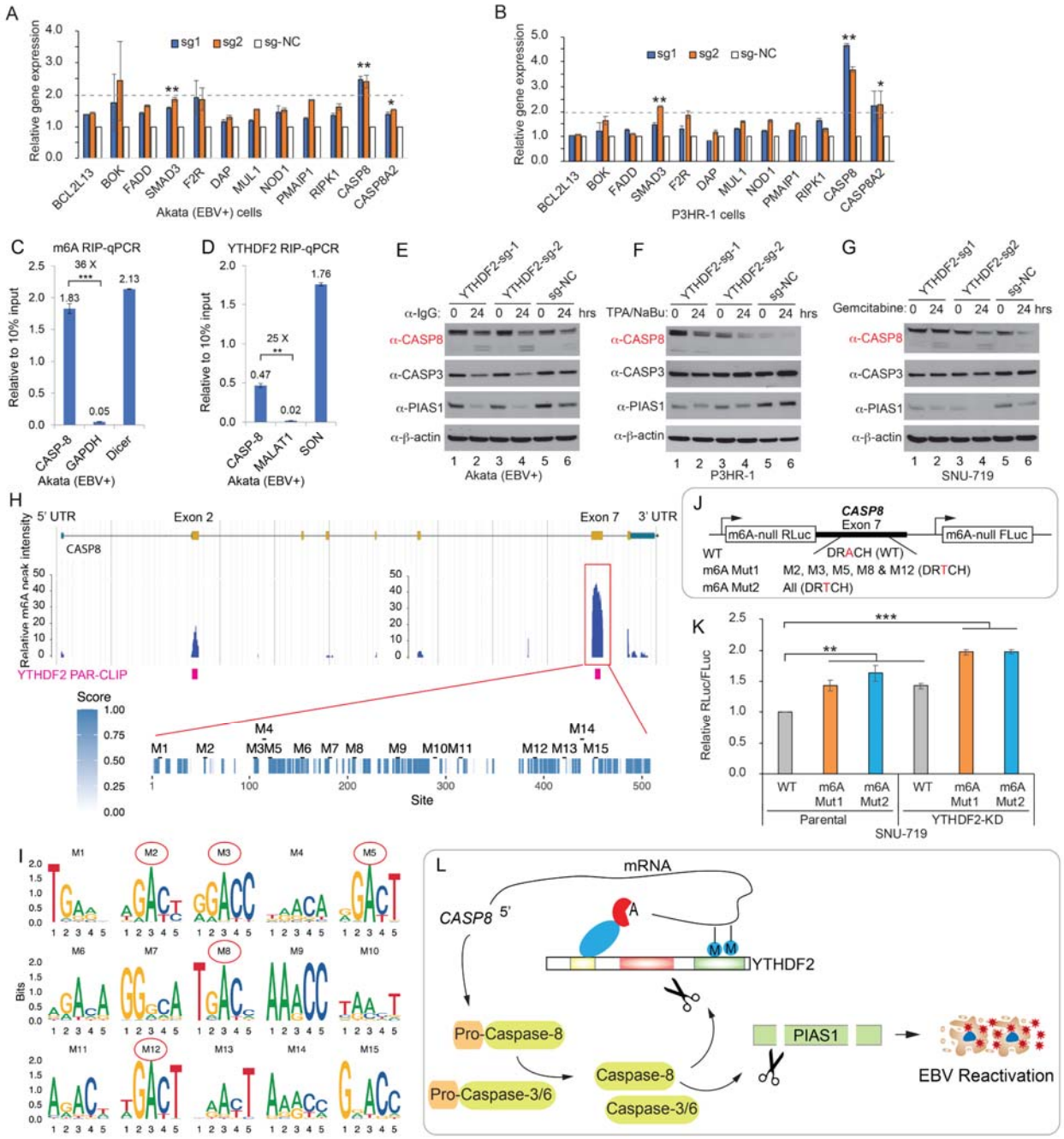

743

744 **Figure 5. YTHDF2 regulates *CASP8* mRNA stability through m^{6}A modifications.**

745 (A-B) YTHDF2 depletion promotes *CASP8* mRNA expression. Akata (EBV+) cells and P3HR-1

746 cells carrying different sgRNA targeting YTHDF2 or control (sg-NC) were used to extract total

747 RNA and qPCR analyses were performed a group of YTHDF2-targeted cellular genes involved

in caspase activation. The values were normalized with a non YTHDF2 target *HPRT1*. The values of sg-NC were set as 1.

(C-D) *CASP8* is modified by m^6A and YTHDF2 binding to *CASP8*. Akata (EBV+) cells were used to perform m6A RIP-qPCR (C) and YTHDF2 RIP-qPCR (D), respectively. Values are displayed as fold change over 10% input.

(E-G) YTHDF2 depletion promotes caspase-8 protein expression and PIAS1 cleavage upon lytic induction. Akata (EBV+) cells (E), P3HR-1 cells (F) and SNU-719 cells (G) carrying different sgRNA targeting YTHDF2 or control (sg-NC) were lytically induced by anti-IgG, TPA and sodium butyrate (NaBu) and gemcitabine treatment for 24 hrs. Protein expression was monitored by Western Blot using antibodies as indicated.

(H) *CASP8* m^6A peaks were extracted from MeT-DB V2.0 database. YTHDF2-PAR-CLIP data were retrieved from Wang et al.(Wang et al., 2014). The Exon-7 of *CASP8* with highest m^6A peaks were analyzed for conservation among sequences derived from 100 vertebrate species. 15 potential m^6A motifs (M1-M15) were extracted based on m^6A motif DRACH.

(I) Motif logos were generated for 15 individual sites. Red cycles denote highly conserved motifs (M2, M3, M5, M8 and M12) across 100 vertebrate species.

(J-K) WT and mutant *CASP8*-Exon-7 were cloned into the m^6A-null Renilla luciferase (RLuc) reporter (3'UTR region) that also express Firefly luciferase (FLuc) from a separate promoter (J). These three reporter plasmids were transfected into parental or YTHDF2-depleted (YTHDF2 KD) SNU719 cells. Relative Renilla to Filefly luciferase activity (RLuc/FLuc) was calculated (K). The value of WT in parental cells was set as 1.

(L) Model illustrating YTHDF2 regulation of *CASP8* mRNA and caspase-8 regulation of YTHDF2 and PIAS1 in EBV reactivation.

Results from three biological replicates are presented. Error bars indicate ±SD. *, $p < 0.05$; **, $p < 0.01$; ***, $p < 0.001$.

See also Figures S3, S4 and Table S3.

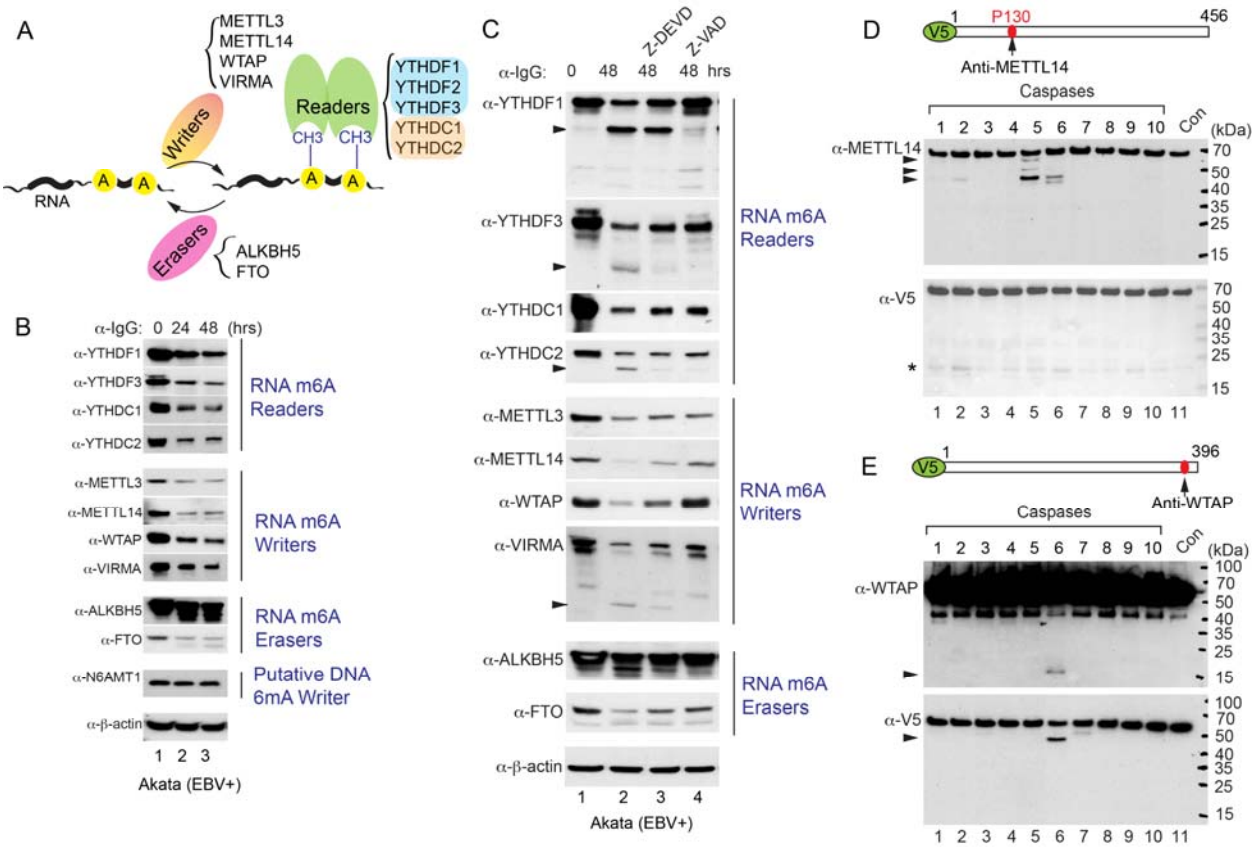

Figure 6. Caspases cleave m^{6}A RNA modification pathway proteins

(A) Diagram summarizing the major writers, readers and erasers involved in the m^{6}A RNA modification pathway.

(B) The downregulation of m^{6}A RNA modification pathway proteins during EBV reactivation. Akata (EBV+) cells was treated with anti-IgG antibody to induce EBV reactivation for 0, 24 and 48 hrs. Western Blot was performed using antibodies as indicated. N6AMT1 and β-actin blots were included as controls.

(C) Caspase inhibition blocks the degradation of m^{6}A RNA modification pathway proteins. The Akata (EBV+) cells were either untreated or pretreated with a caspase-3/-7 inhibitor (Z-DEVD-FMK, 50 μM) or pan-caspase inhibitor (Z-VAD-FMK, 50 μM) for 1 hr, and then anti-IgG antibody was added for 48 hrs. Western Blot was performed using antibodies as indicated.

(D and E) V5-METTL14 (D) and V5-WTAP (E) were incubated with individual caspase for 2 hrs at 37°C. Western Blot was performed using anti-METTL14, anti-V5 and anti-WTAP antibodies as indicated. The locations of antibody recognition epitopes were labelled as indicated. Arrowheads denote cleaved fragments. Star denotes non-specific bands.

See also Figures S5-S7.

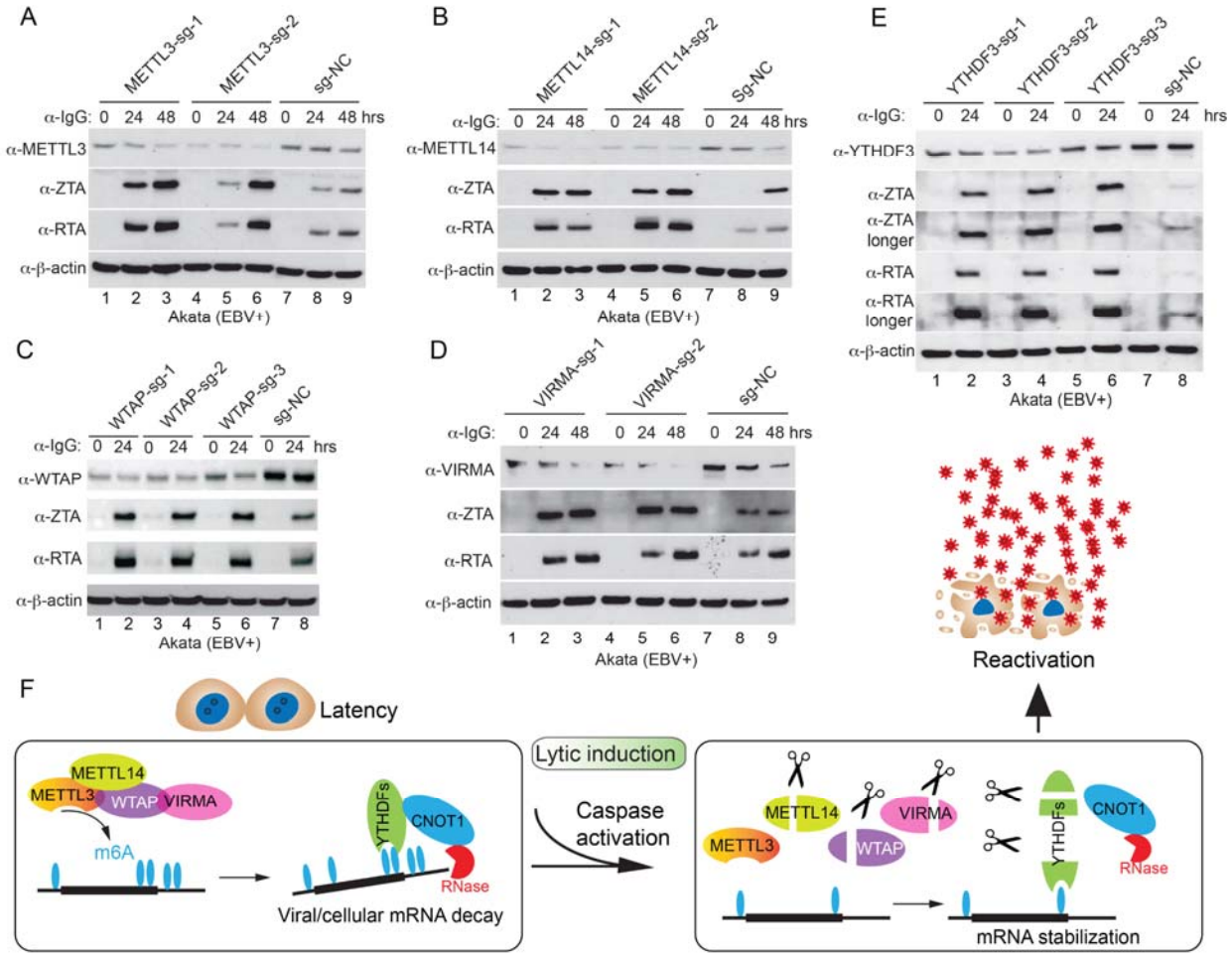

Figure 7. Depletion of m^{6}A writers and reader YTHDF3 promotes EBV reactivation.

(A-E) Akata (EBV+) cells were used to establish stable cell lines using 2-3 different guide RNA constructs targeting METTL3 (A), METTL14 (B), WTAP (C), VIRMA (D) and YTHDF3 (E) and a non-targeting control (sg-NC). The cells were untreated or lytically induced with anti-IgG-mediated BCR activation. Cellular and viral protein expression levels were monitored by Western Blot using antibodies as indicated.

(F) Model summarizing the regulation of m^{6}A RNA modification pathway in EBV life cycle. During latency, m^{6}A writers deposit the methyl group onto key viral and cellular mRNAs which are subsequently destabilized by m^{6}A readers. Upon reactivation, on one hand, cellular caspases cleave the writers to limit the m^{6}A modification process, and on the other hand, caspases cleave

readers to limits RNA decay by CNOT-CCR4 complex, which together drive the production of massive amounts of viruses.

See also Figure S7.

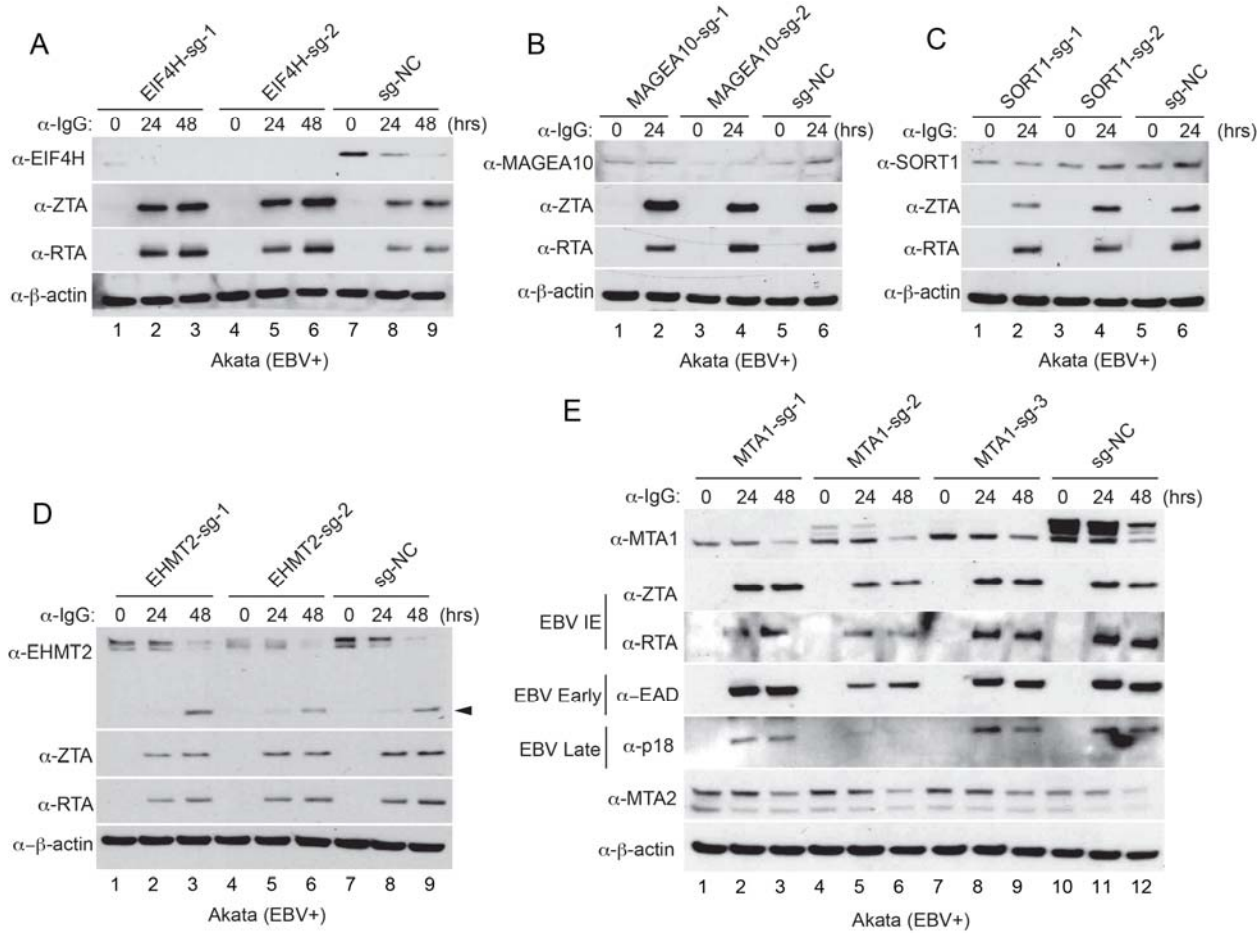

Figure S1. The role of EIF4H, MAGEA10, SORT1, EHMT2, and MTA1 during EBV lytic induction. See also Figure 2.

(A-E) Akata (EBV+) cells were used to establish stable cell lines using 2 or 3 different sgRNA constructs and a non-targeting control (sg-NC). The cells were untreated or lytically induced with anti-IgG treatment for 24 or 48 hrs as indicated. Cellular and viral protein expression levels were monitored by Western Blot using antibodies as indicated.

(A) EIF4H depletion promotes the expression of EBV ZTA and RTA.

(B) MAGEA10 depletion does not affect EBV protein expression.

(C) SORT1 depletion does not significantly affect EBV protein expression.

(D) EHMT2 depletion does not affect EBV protein expression.

(E) MTA1 depletion does not uniformly affect EBV protein expression but slightly enhances the expression of its homolog MTA2.

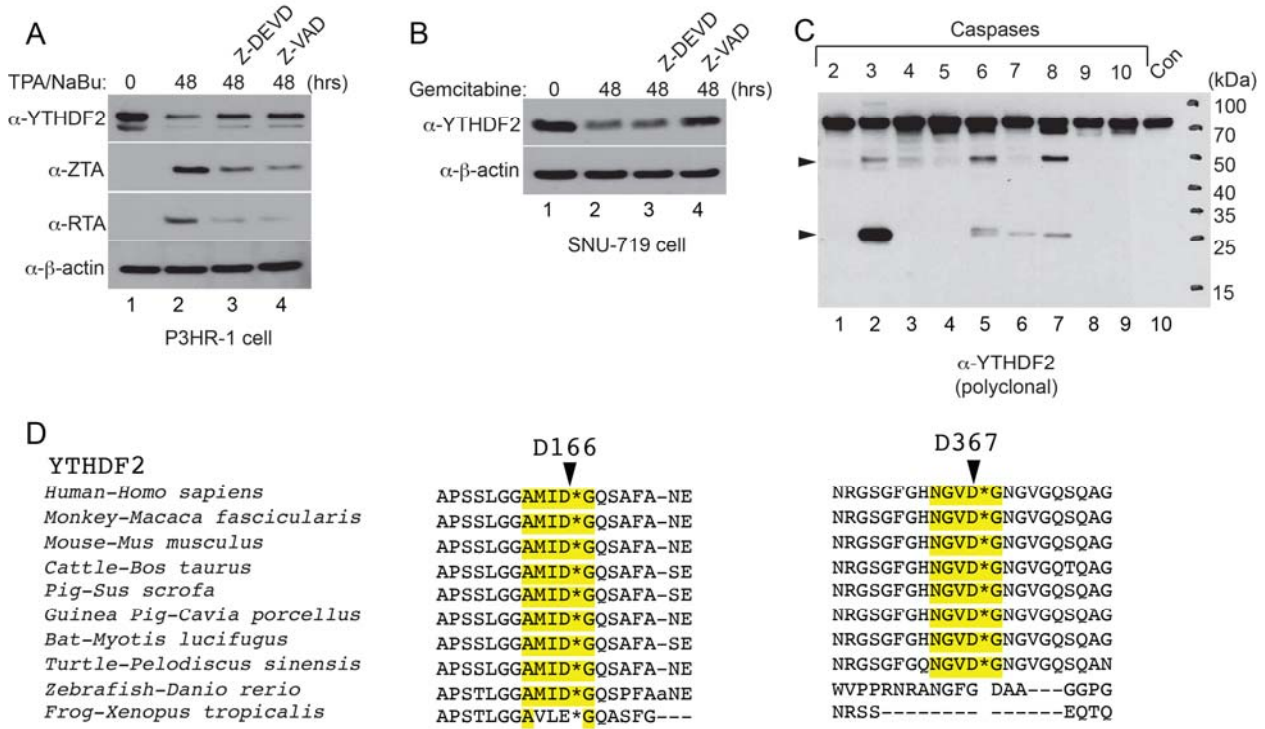

Figure S2. See also Figure 3 and Table S2.

(A) Caspase inhibition blocks YTHDF2 degradation and viral protein expression. P3HR-1 cells were either untreated or pretreated with caspase-3 (Z-DEVD-FMK) or pan-caspase inhibitors (Z-VAD-FMK) (50 μM) for 1 hr and then lytically induced by TPA and sodium butyrate (NaBu) for 48 hrs, Protein levels were monitored by Western Blot as indicated.

(B) Caspase inhibition blocks YTHDF2 degradation in SNU-719 cells. SNU-719 cells were either untreated or pretreated with caspase-3 or pan-caspase inhibitors (50 μM) for 1 hr and then lytically induced by gemcitabine (1 μg/ml) for 48 hrs, Protein levels were monitored by antibodies as indicated.

(C) Recombinant wild-type YTHDF2 was incubated with individual caspases for 2 hr at 37°C. Western Blot analysis showing YTHDF2 cleavage by caspase-3, -6, -8 and to a lesser extent, caspase-7. Arrowheads denote cleavage fragments.

(D) Sequence alignment of YTHDF2 sequences from 10 representative species using the Constraint-based Multiple Alignment Tool (COBALT). The cleavage motifs were highlighted by yellow color.

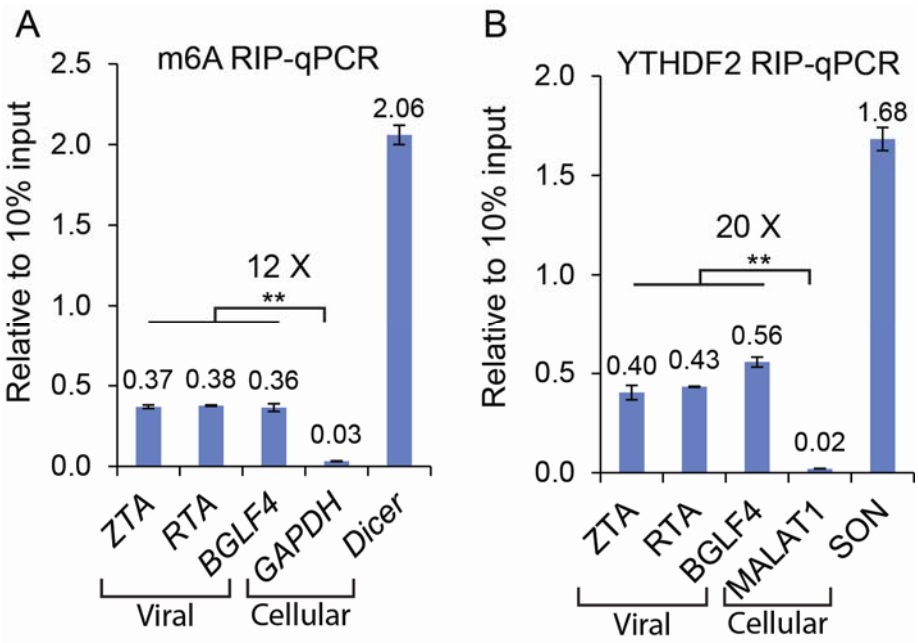

Figure S3. YTHDF2 binds to EBV transcripts and viral RNAs contain m^{6}A modifications. See also Figure 5.

Akata (EBV+) cells were lytically induced by IgG-cross linking for 24 hrs.

(A) Total RNA was subjected to m^{6}A RIP, followed by RT-qPCR using indicated primers. Values are displayed as fold change over 10% input. GAPDH and Dicer are cellular negative and positive controls, respectively.

(B) Cell lysate was collected to detect YTHDF2 binding of viral RNAs by RIP-qPCR. Values are displayed as fold change over 10% input. MALAT1 and SON are cellular negative and positive controls, respectively.

Results from three biological replicates are presented. Error bars indicate ±SD. **, $p < 0.01$.

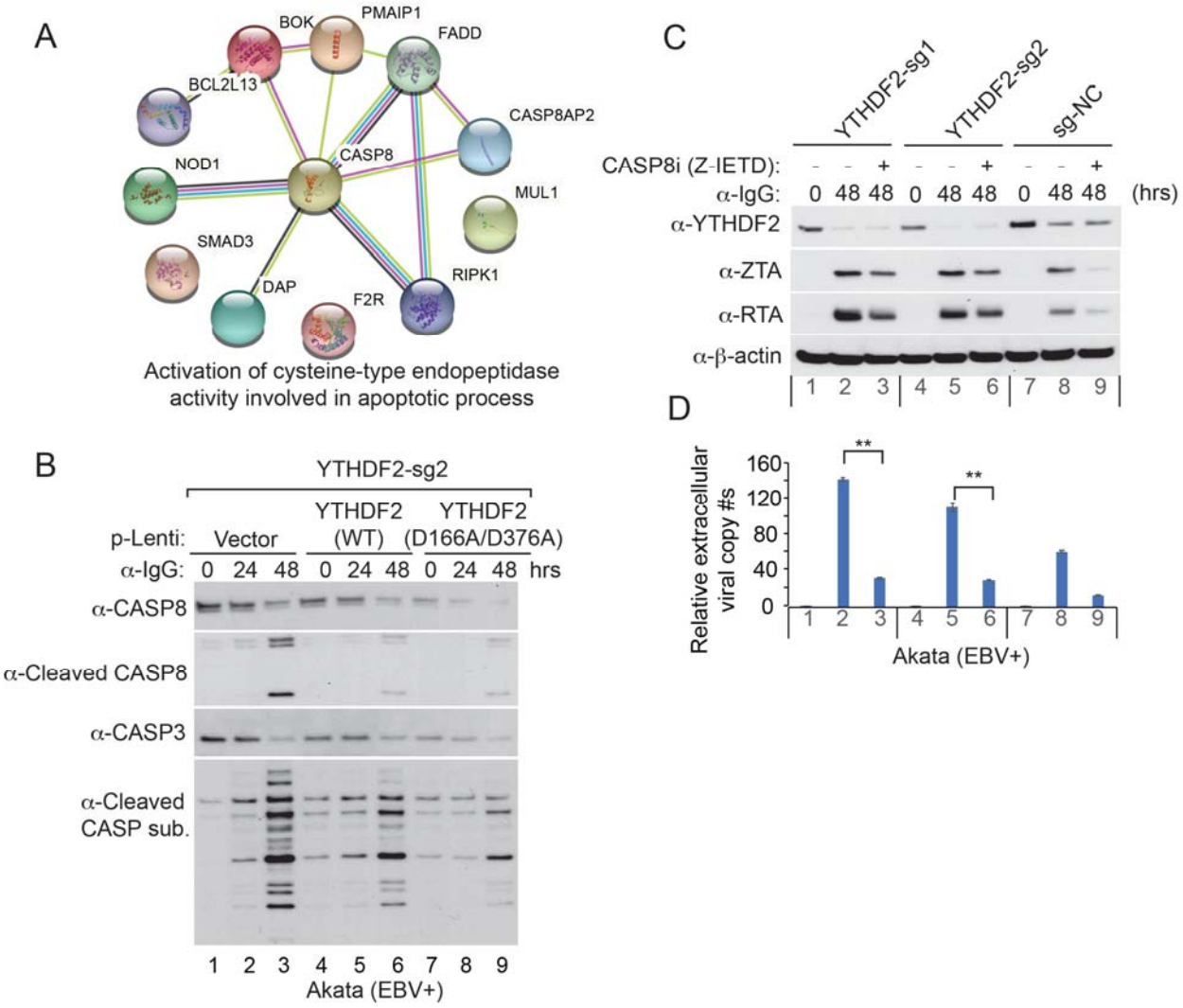

Figure S4. See also Figures 4 and 5.

(A) A group of genes in the category of "*activation of cysteine-type endopeptidase activity involved in apoptotic process*" (also called "*caspase activation*") were extracted from YTHDF2 target genes derived from YTHDF2 RIP-seq and PAR-CLIP-seq datasets (Liu et al., 2015; Liu et al., 2018; Wang et al., 2014)

(B) YTHDF2 reconstitution suppresses caspase-8 expression and subsequent caspase activation. Akata (EBV+) YTHDF2-sg2 cells were reconstituted with WT or cleavage-resistant YTHDF2 (D166A/D367A) using lentiviral constructs. Western Blot analysis showing the levels for

caspase-8 (CASP8), cleaved caspase-8, caspase-3 (CASP3) and cleaved caspase substrates (CASP sub.) in these cell lines upon IgG cross-linking as indicated.

(C-D) Caspase-8 inhibition suppress EBV replication in YTHDF2-depleted cells. Control and YTHDF2-depleted Akata (EBV+) cells were either untreated or pretreated with caspase-8 inhibitor (Z-IETD-FMK, 50 μM) for 1 hr and then anti-IgG antibody was added for 0 to 48 hrs. Western Blot showing the protein levels of EBV ZTA and RTA as indicated (C). Extracellular viral DNA was measured by qPCR using primers specific to BALF5 (D). The value of vector control at 0 hr was set as 1. Results from three biological replicates are presented. Error bars indicate ±SD. **, $p<0.01$.

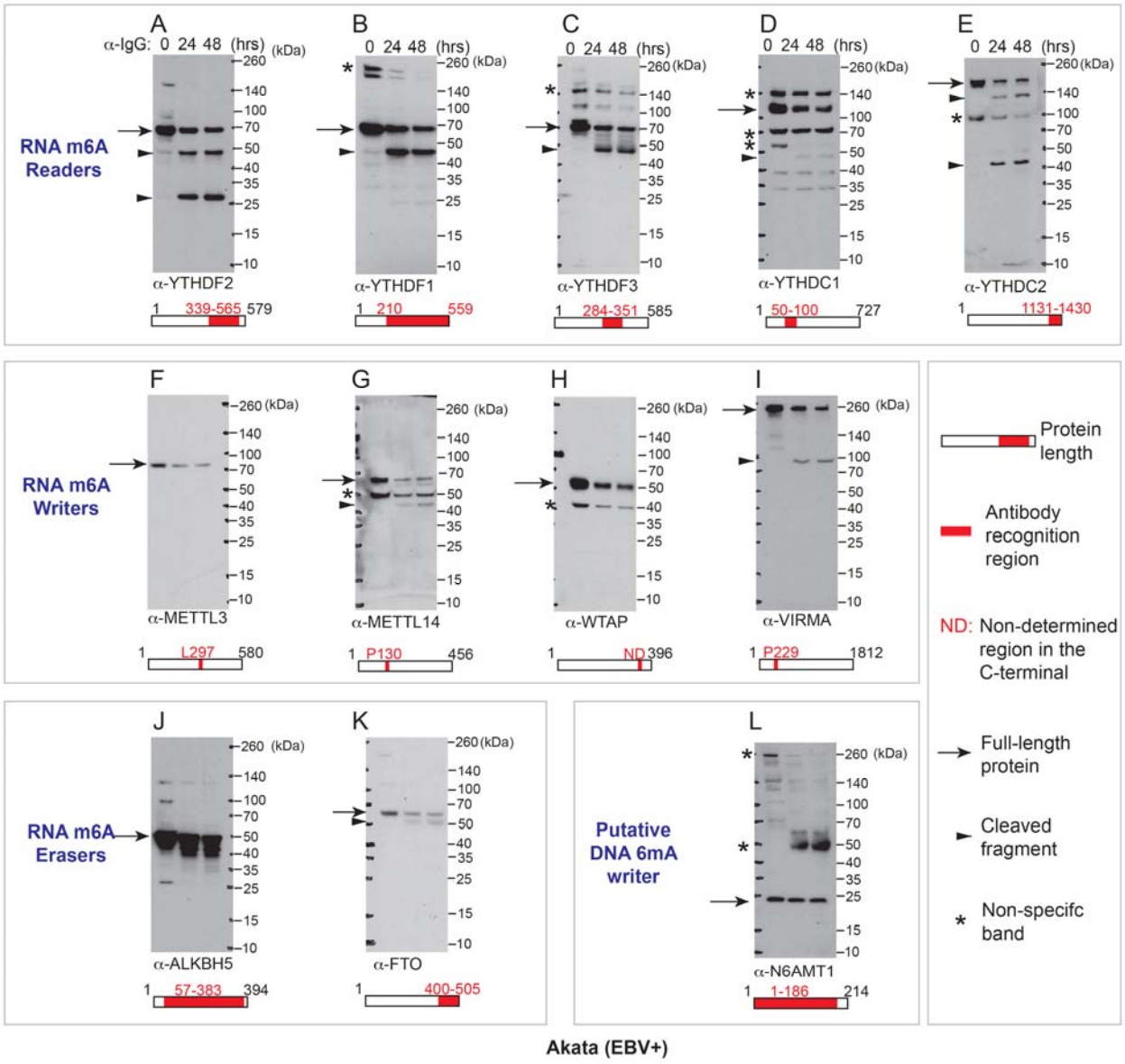

Figure S5. See also Figure 6.

Full blots from Figure 6B showing the generation of cleaved fragments for m^6A readers, writers and erasers. Western Blot was performed using antibodies as indicated. N6AMT1 blot was included as a control.

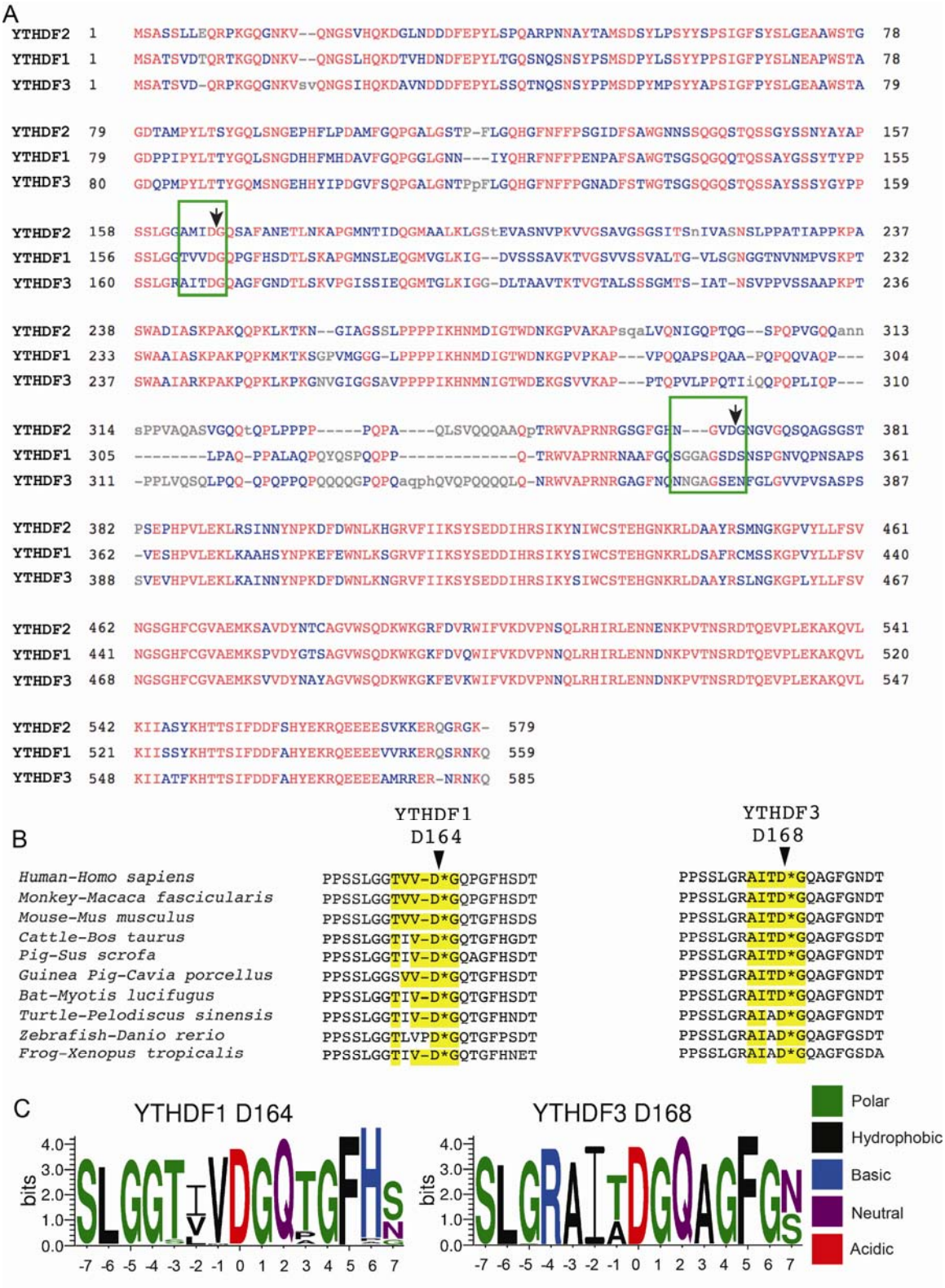

Figure S6. See also Figure 6 and Table S2.

(A) Sequence alignment of YTHDF2 with YTHDF1 and YTHDF2 s using the Constraint-based Multiple Alignment Tool (COBALT). The corresponding cleavage motifs were highlighted by green boxes.

(B) Sequence alignment of YTHDF2 sequences from 10 representative species using the Constraint-based Multiple Alignment Tool (COBALT). The cleavage motifs were highlighted by yellow color.

(C) Motif analysis showing the conservation of YTHDF1-D164/YTHDF3-D168 and the surrounding amino acids. Amino acid sequences were extracted from 97 vertebrate species and motif logos were generated using WebLogo.

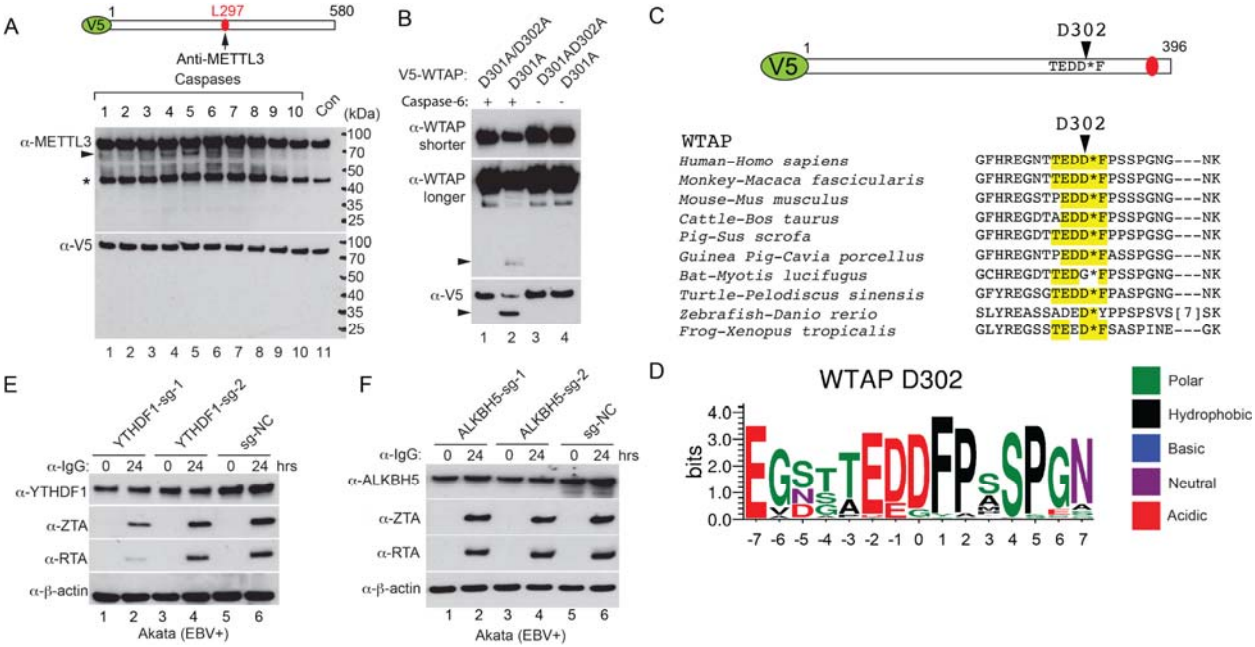

Figure S7. See also Figures 6, 7 and Table S2.

(A) V5-METTL3 was incubated with individual caspase for 2 hrs at 37°C. Western Blot was performed using anti-METTL3 and anti-V5 antibodies as indicated. The locations of antibody recognition epitopes were labelled as indicated. The positions of weakly cleaved fragments were labelled by arrowhead. Star denotes non-specific bands.

(B) V5-tagged WTAP D301A/D302A and D301A mutants were incubated with individual recombinant caspase for 2 hrs. Western Blot was performed using antibodies as indicated. Arrowheads denote cleaved fragments.

(C) Sequence alignment of WTAP sequences from 10 representative species using the Constraint-based Multiple Alignment Tool (COBALT). The cleavage motifs were highlighted by yellow color.

(D) Motif analysis showing the conservation of the WTAP D302 and the surrounding amino acids. Amino acid sequences were extracted from 97 vertebrate species and motif logos were generated using WebLogo.

(E-F) Akata (EBV+) cells were used to establish stable cell lines using 2 different guide RNA constructs targeting YTHDF1 (D) and ALKBH5 (E) and a non-targeting control (sg-NC). The cells were untreated or lytically induced with anti-IgG-mediated BCR activation. Cellular and viral protein expression levels were monitored by Western Blot using antibodies as indicated.

Acknowledgements

We thank S. Diane Hayward (Johns Hopkins) for providing reagent and cells lines. We thank Stacy Horner (Duke University) for providing a dual luciferase reporter plasmid. We thank Feng Zhang (MIT/Broad), Mohan Babu (University of Regina) and Joshua Mendell (University of Texas Southwestern Medical Center) for sharing the lentiCRISPR v2 plasmids. We also thank Didier Trono (EPFL) for providing the pMD2.G and psPAX2 plasmids.

Funding Information

This work was in part supported by grants from the National Institute of Allergy and Infectious Diseases (AI104828 and AI141410; https://grants.nih.gov/grants/oer.htm). The work was also supported by Institutional Research Grant (IRG-14-192-40) and Research Scholar Grant (134703-RSG-20-054-01-MPC) from the American Cancer Society, and Massey Cancer Center CMG program Mini-project Grant. R.L. received support from the VCU Philips Institute for Oral Health Research, the VCU NCI Designated Massey Cancer Center (NIH P30 CA016059) (https://grants.nih.gov/grants/oer.htm), and the VCU Presidential Quest for Distinction Award. J. W. had support from Indiana University Simon Cancer Center (NIH P30 CA082709). The funders had no role in study design, data collection and analysis, decision to publish, or preparation of the manuscript.

Author Contributions

Conceptualization, R.L. and K.Z.; Methodology, K.Z., R.L., Y.Z. and J.W.; Investigation, K.Z., R.L., Y.Z. and J.W,; Writing – Original Draft, R.L. and K.Z.; Writing – Review & Editing, K.Z.,

R.L., Y.Z. and J.W.; Funding Acquisition, R.L., Y.Z. and J.W.; Visualization, K.Z., R.L., Y.Z. and J.W.; Supervision, R.L., and J.W.

References

Burton, E.M., Goldbach-Mansky, R., and Bhaduri-McIntosh, S. (2020). A promiscuous inflammasome sparks replication of a common tumor virus. Proceedings of the National Academy of Sciences of the United States of America *117*, 1722-1730.

Cohen, J.I., Fauci, A.S., Varmus, H., and Nabel, G.J. (2011). Epstein-Barr virus: an important vaccine target for cancer prevention. Sci Transl Med *3*, 107fs107.

Courtney, D.G., Kennedy, E.M., Dumm, R.E., Bogerd, H.P., Tsai, K., Heaton, N.S., and Cullen, B.R. (2017). Epitranscriptomic Enhancement of Influenza A Virus Gene Expression and Replication. Cell host & microbe *22*, 377-386 e375.

Crooks, G.E., Hon, G., Chandonia, J.M., and Brenner, S.E. (2004). WebLogo: a sequence logo generator. Genome Res *14*, 1188-1190.

De Leo, A., Calderon, A., and Lieberman, P.M. (2020). Control of Viral Latency by Episome Maintenance Proteins. Trends Microbiol *28*, 150-162.

De Leo, A., Chen, H.S., Hu, C.A., and Lieberman, P.M. (2017). Deregulation of KSHV latency conformation by ER-stress and caspase-dependent RAD21-cleavage. PLoS Pathog *13*, e1006596.

Dominissini, D., Moshitch-Moshkovitz, S., Schwartz, S., Salmon-Divon, M., Ungar, L., Osenberg, S., Cesarkas, K., Jacob-Hirsch, J., Amariglio, N., Kupiec, M.*, et al.* (2012). Topology of the human and mouse m6A RNA methylomes revealed by m6A-seq. Nature *485*, 201-206.

Du, H., Zhao, Y., He, J., Zhang, Y., Xi, H., Liu, M., Ma, J., and Wu, L. (2016). YTHDF2 destabilizes m(6)A-containing RNA through direct recruitment of the CCR4-NOT deadenylase complex. Nature communications *7*, 12626.

Fei, Q., Zou, Z., Roundtree, I.A., Sun, H.L., and He, C. (2020). YTHDF2 promotes mitotic entry and is regulated by cell cycle mediators. PLoS Biol *18*, e3000664.

Fu, D.X., Tanhehco, Y., Chen, J., Foss, C.A., Fox, J.J., Chong, J.M., Hobbs, R.F., Fukayama, M., Sgouros, G., Kowalski, J.*, et al.* (2008). Bortezomib-induced enzyme-targeted radiation therapy in herpesvirus-associated tumors. Nature medicine *14*, 1118-1122.

Fu, Y., and Zhuang, X. (2020). m(6)A-binding YTHDF proteins promote stress granule formation. Nature chemical biology *16*, 955-963.

Gokhale, N.S., McIntyre, A.B.R., Mattocks, M.D., Holley, C.L., Lazear, H.M., Mason, C.E., and Horner, S.M. (2020). Altered m(6)A Modification of Specific Cellular Transcripts Affects Flaviviridae Infection. Molecular cell *77*, 542-555 e548.

Gokhale, N.S., McIntyre, A.B.R., McFadden, M.J., Roder, A.E., Kennedy, E.M., Gandara, J.A., Hopcraft, S.E., Quicke, K.M., Vazquez, C., Willer, J.*, et al.* (2016). N6-Methyladenosine in Flaviviridae Viral RNA Genomes Regulates Infection. Cell host & microbe *20*, 654-665.

Golden, R.J., Chen, B., Li, T., Braun, J., Manjunath, H., Chen, X., Wu, J., Schmid, V., Chang, T.C., Kopp, F.*, et al.* (2017). An Argonaute phosphorylation cycle promotes microRNA-mediated silencing. Nature *542*, 197-202.

Hesser, C.R., Karijolich, J., Dominissini, D., He, C., and Glaunsinger, B.A. (2018). N6-methyladenosine modification and the YTHDF2 reader protein play cell type specific roles in lytic viral gene expression during Kaposi's sarcoma-associated herpesvirus infection. PLoS pathogens *14*, e1006995.

Hubisz, M.J., Pollard, K.S., and Siepel, A. (2011). PHAST and RPHAST: phylogenetic analysis with space/time models. Brief Bioinform *12*, 41-51.

Imam, H., Khan, M., Gokhale, N.S., McIntyre, A.B.R., Kim, G.W., Jang, J.Y., Kim, S.J., Mason, C.E., Horner, S.M., and Siddiqui, A. (2018). N6-methyladenosine modification of hepatitis B virus RNA differentially regulates the viral life cycle. Proceedings of the National Academy of Sciences of the United States of America *115*, 8829-8834.

Jia, G., Fu, Y., Zhao, X., Dai, Q., Zheng, G., Yang, Y., Yi, C., Lindahl, T., Pan, T., Yang, Y.G.*, et al.* (2011). N6-methyladenosine in nuclear RNA is a major substrate of the obesity-associated FTO. Nature chemical biology *7*, 885-887.

Julien, O., and Wells, J.A. (2017). Caspases and their substrates. Cell Death Differ *24*, 1380-1389.

Kennedy, E.M., Bogerd, H.P., Kornepati, A.V., Kang, D., Ghoshal, D., Marshall, J.B., Poling, B.C., Tsai, K., Gokhale, N.S., Horner, S.M.*, et al.* (2016). Posttranscriptional m(6)A Editing of HIV-1 mRNAs Enhances Viral Gene Expression. Cell host & microbe *19*, 675-685.

Kenney, S.C., and Mertz, J.E. (2014). Regulation of the latent-lytic switch in Epstein-Barr virus. Semin Cancer Biol *26*, 60-68.

Kumar, S., van Raam, B.J., Salvesen, G.S., and Cieplak, P. (2014). Caspase cleavage sites in the human proteome: CaspDB, a database of predicted substrates. PloS one *9*, e110539.

Lang, F., Singh, R.K., Pei, Y., Zhang, S., Sun, K., and Robertson, E.S. (2019). EBV epitranscriptome reprogramming by METTL14 is critical for viral-associated tumorigenesis. PLoS pathogens *15*, e1007796.

Lasman, L., Krupalnik, V., Viukov, S., Mor, N., Aguilera-Castrejon, A., Schneir, D., Bayerl, J., Mizrahi, O., Peles, S., Tawil, S.*, et al.* (2020). Context-dependent functional compensation between Ythdf m(6)A reader proteins. Genes & development.

987 Li, F., Zhao, D., Wu, J., and Shi, Y. (2014). Structure of the YTH domain of human YTHDF2 in
988 complex with an m(6)A mononucleotide reveals an aromatic cage for m(6)A recognition. Cell
989 research *24*, 1490-1492.
990 Li, R., Liao, G., Nirujogi, R.S., Pinto, S.M., Shaw, P.G., Huang, T.C., Wan, J., Qian, J., Gowda, H.,
991 Wu, X.*, et al.* (2015). Phosphoproteomic Profiling Reveals Epstein-Barr Virus Protein Kinase
992 Integration of DNA Damage Response and Mitotic Signaling. PLoS pathogens *11*, e1005346.
993 Lichinchi, G., Zhao, B.S., Wu, Y., Lu, Z., Qin, Y., He, C., and Rana, T.M. (2016). Dynamics of
994 Human and Viral RNA Methylation during Zika Virus Infection. Cell host & microbe *20*, 666-673.
995 Lieberman, P.M. (2013). Keeping it quiet: chromatin control of gammaherpesvirus latency. Nat
996 Rev Microbiol *11*, 863-875.
997 Linder, B., Grozhik, A.V., Olarerin-George, A.O., Meydan, C., Mason, C.E., and Jaffrey, S.R. (2015).
998 Single-nucleotide-resolution mapping of m6A and m6Am throughout the transcriptome. Nature
999 methods *12*, 767-772.
1000 Liu, H., Flores, M.A., Meng, J., Zhang, L., Zhao, X., Rao, M.K., Chen, Y., and Huang, Y. (2015).
1001 MeT-DB: a database of transcriptome methylation in mammalian cells. Nucleic acids research
1002 *43*, D197-203.
1003 Liu, H., Wang, H., Wei, Z., Zhang, S., Hua, G., Zhang, S.W., Zhang, L., Gao, S.J., Meng, J., Chen, X.*,*
1004 *et al.* (2018). MeT-DB V2.0: elucidating context-specific functions of N6-methyl-adenosine
1005 methyltranscriptome. Nucleic acids research *46*, D281-D287.
1006 Liu, J., Yue, Y., Han, D., Wang, X., Fu, Y., Zhang, L., Jia, G., Yu, M., Lu, Z., Deng, X.*, et al.* (2014). A
1007 METTL3-METTL14 complex mediates mammalian nuclear RNA N6-adenosine methylation.
1008 Nature chemical biology *10*, 93-95.

1009 Lv, D.W., Zhang, K., and Li, R. (2018). Interferon regulatory factor 8 regulates caspase-1
1010 expression to facilitate Epstein-Barr virus reactivation in response to B cell receptor stimulation
1011 and chemical induction. PLoS pathogens *14*, e1006868.
1012 Lv, D.W., Zhong, J., Zhang, K., Pandey, A., and Li, R. (2017). Understanding Epstein-Barr Virus
1013 Life Cycle with Proteomics: A Temporal Analysis of Ubiquitination During Virus Reactivation.
1014 OMICS: A Journal of Integrative Biology *21*, 27-37.
1015 Mahrus, S., Trinidad, J.C., Barkan, D.T., Sali, A., Burlingame, A.L., and Wells, J.A. (2008). Global
1016 sequencing of proteolytic cleavage sites in apoptosis by specific labeling of protein N termini.
1017 Cell *134*, 866-876.
1018 Manners, O., Baquero-Perez, B., and Whitehouse, A. (2018). m(6)A: Widespread regulatory
1019 control in virus replication. Biochimica et biophysica acta Gene regulatory mechanisms.
1020 Meyer, K.D., and Jaffrey, S.R. (2017). Rethinking m(6)A Readers, Writers, and Erasers. Annual
1021 review of cell and developmental biology *33*, 319-342.
1022 Meyer, K.D., Saletore, Y., Zumbo, P., Elemento, O., Mason, C.E., and Jaffrey, S.R. (2012).
1023 Comprehensive analysis of mRNA methylation reveals enrichment in 3' UTRs and near stop
1024 codons. Cell *149*, 1635-1646.
1025 Pettersen, E.F., Goddard, T.D., Huang, C.C., Couch, G.S., Greenblatt, D.M., Meng, E.C., and
1026 Ferrin, T.E. (2004). UCSF Chimera--a visualization system for exploratory research and analysis. J
1027 Comput Chem *25*, 1605-1612.
1028 Ries, R.J., Zaccara, S., Klein, P., Olarerin-George, A., Namkoong, S., Pickering, B.F., Patil, D.P.,
1029 Kwak, H., Lee, J.H., and Jaffrey, S.R. (2019). m(6)A enhances the phase separation potential of
1030 mRNA. Nature *571*, 424-428.

1031 Rubio, R.M., Depledge, D.P., Bianco, C., Thompson, L., and Mohr, I. (2018). RNA m(6) A
1032 modification enzymes shape innate responses to DNA by regulating interferon beta. Genes &
1033 development *32*, 1472-1484.
1034 Sanjana, N.E., Shalem, O., and Zhang, F. (2014). Improved vectors and genome-wide libraries for
1035 CRISPR screening. Nat Methods *11*, 783-784.
1036 Shi, H., Wang, X., Lu, Z., Zhao, B.S., Ma, H., Hsu, P.J., Liu, C., and He, C. (2017). YTHDF3 facilitates
1037 translation and decay of N(6)-methyladenosine-modified RNA. Cell research *27*, 315-328.
1038 Tabtieng, T., Degterev, A., and Gaglia, M.M. (2018). Caspase-Dependent Suppression of Type I
1039 Interferon Signaling Promotes Kaposi's Sarcoma-Associated Herpesvirus Lytic Replication.
1040 Journal of virology *92*.
1041 Tan, B., and Gao, S.J. (2018). The RNA Epitranscriptome of DNA Viruses. Journal of virology *92*.
1042 Tan, B., Liu, H., Zhang, S., da Silva, S.R., Zhang, L., Meng, J., Cui, X., Yuan, H., Sorel, O., Zhang,
1043 S.W.*, et al.* (2018). Viral and cellular N(6)-methyladenosine and N(6),2'-O-dimethyladenosine
1044 epitranscriptomes in the KSHV life cycle. Nature microbiology *3*, 108-120.
1045 Tirumuru, N., Zhao, B.S., Lu, W., Lu, Z., He, C., and Wu, L. (2016). N(6)-methyladenosine of HIV-1
1046 RNA regulates viral infection and HIV-1 Gag protein expression. eLife *5*.
1047 Tsai, K., Courtney, D.G., and Cullen, B.R. (2018). Addition of m6A to SV40 late mRNAs enhances
1048 viral structural gene expression and replication. PLoS pathogens *14*, e1006919.
1049 Wagih, O. (2017). ggseqlogo: a versatile R package for drawing sequence logos. Bioinformatics
1050 *33*, 3645-3647.
1051 Wang, J., Wang, L., Diao, J., Shi, Y.G., Shi, Y., Ma, H., and Shen, H. (2020). Binding to m(6)A RNA
1052 promotes YTHDF2-mediated phase separation. Protein Cell *11*, 304-307.

1053 Wang, X., Lu, Z., Gomez, A., Hon, G.C., Yue, Y., Han, D., Fu, Y., Parisien, M., Dai, Q., Jia, G.*, et al.*
1054 (2014). N6-methyladenosine-dependent regulation of messenger RNA stability. Nature *505*,
1055 117-120.
1056 Williams, G.D., Gokhale, N.S., and Horner, S.M. (2019). Regulation of Viral Infection by the RNA
1057 Modification N6-methyladenosine. Annual review of virology *29*, 235-253.
1058 Winkler, R., Gillis, E., Lasman, L., Safra, M., Geula, S., Soyris, C., Nachshon, A., Tai-Schmiedel, J.,
1059 Friedman, N., Le-Trilling, V.T.K.*, et al.* (2018). m(6)A modification controls the innate immune
1060 response to infection by targeting type I interferons. Nature immunology.
1061 Yang, J., and Zhang, Y. (2015). I-TASSER server: new development for protein structure and
1062 function predictions. Nucleic acids research *43*, W174-181.
1063 Young, L.S., and Rickinson, A.B. (2004). Epstein-Barr virus: 40 years on. Nat Rev Cancer *4*, 757-
1064 768.
1065 Young, L.S., Yap, L.F., and Murray, P.G. (2016). Epstein-Barr virus: more than 50 years old and
1066 still providing surprises. Nat Rev Cancer *16*, 789-802.
1067 Zaccara, S., and Jaffrey, S.R. (2020). A Unified Model for the Function of YTHDF Proteins in
1068 Regulating m(6)A-Modified mRNA. Cell *181*, 1582-1595 e1518.
1069 Zhang, C., Freddolino, P.L., and Zhang, Y. (2017a). COFACTOR: improved protein function
1070 prediction by combining structure, sequence and protein-protein interaction information.
1071 Nucleic acids research *45*, W291-W299.
1072 Zhang, K., Lv, D.W., and Li, R. (2017b). B Cell Receptor Activation and Chemical Induction Trigger
1073 Caspase-Mediated Cleavage of PIAS1 to Facilitate Epstein-Barr Virus Reactivation. Cell reports
1074 *21*, 3445-3457.

Zhang, K., Lv, D.W., and Li, R. (2019). Conserved Herpesvirus Protein Kinases Target SAMHD1 to Facilitate Virus Replication. Cell reports *28*, 449-459 e445.

Zheng, G., Dahl, J.A., Niu, Y., Fedorcsak, P., Huang, C.M., Li, C.J., Vagbo, C.B., Shi, Y., Wang, W.L., Song, S.H.*, et al.* (2013). ALKBH5 is a mammalian RNA demethylase that impacts RNA metabolism and mouse fertility. Molecular cell *49*, 18-29.

Zhu, T., Roundtree, I.A., Wang, P., Wang, X., Wang, L., Sun, C., Tian, Y., Li, J., He, C., and Xu, Y. (2014). Crystal structure of the YTH domain of YTHDF2 reveals mechanism for recognition of N6-methyladenosine. Cell research *24*, 1493-1496.